AFGL-TR-87-0094

④

AD-A200 957

A Projectile Probe for Measuring the
Electric Field Inside a Spacecraft Plasma Sheath

Mark N. Horenstein
Gary Freeman


Boston University
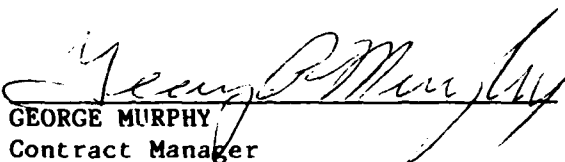110 Cummington Street
Boston, MA 02215

3 March 1987


Final Report
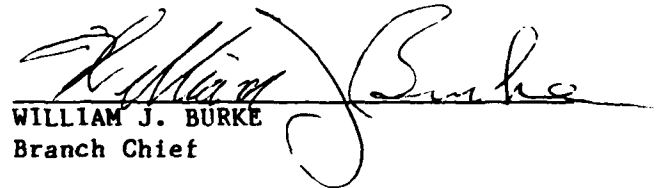14 February 1984 – 3 March 1987


Approved for public release; distribution unlimited

8 8 12

"This technical report has been reviewed and is approved for publication"


GEORGE MURPHY
Contract Manager

WILLIAM J. BURKE
Branch Chief


FOR THE COMMANDER


RITA C. SAGALYN
Division Director


This report has been reviewed by the ESD Public Affairs Office (PA) and is releasable to the National Technical Information Service (NTIS).


Qualified requestors may obtain additional copies from the Defense Technical Information Center.  All others should apply to the National Technical Information Service.


If your address has changed, or if you wish to be removed from the mailing list, or if the addressee is no longer employed by your organization, please notify AFGL/DAA, Hanscom AFB, MA 01731.  This will assist us in maintaining a current mailing list.


Do not return copies of this report unless contractual obligations or notices on a specific document requires that it be returned.

*AD H266 957*

# REPORT DOCUMENTATION PAGE

| 1a. REPORT SECURITY CLASSIFICATION | 1b. RESTRICTIVE MARKINGS |
|---|---|
| UNCLASSIFIED | |

| 2a. SECURITY CLASSIFICATION AUTHORITY | 3. DISTRIBUTION/AVAILABILITY OF REPORT |
|---|---|
| | Approved for public release; Distribution |
| 2b. DECLASSIFICATION/DOWNGRADING SCHEDULE | Unlimited |

| 4. PERFORMING ORGANIZATION REPORT NUMBER(S) | 5. MONITORING ORGANIZATION REPORT NUMBER(S) |
|---|---|
| | AFGL-TR-87-0094 |

| 6a. NAME OF PERFORMING ORGANIZATION | 6b. OFFICE SYMBOL (If applicable) | 7a. NAME OF MONITORING ORGANIZATION |
|---|---|---|
| BOSTON University | | Air Force Geophysics Laboratory |

| 6c. ADDRESS (City, State, and ZIP Code) | 7b. ADDRESS (City, State, and ZIP Code) |
|---|---|
| 110 Cummington Street Boston, MA 02215 | Hanscom AFB Massachusettes 01731 |

| 8a. NAME OF FUNDING/SPONSORING ORGANIZATION | 8b. OFFICE SYMBOL (If applicable) | 9 PROCUREMENT INSTRUMENT IDENTIFICATION NUMBER |
|---|---|---|
| Air Force Syst.Cmd. /ESD | | F19628-84-K0033 |

| 8c. ADDRESS (City, State, and ZIP Code) | 10. SOURCE OF FUNDING NUMBERS | | | |
|---|---|---|---|---|
| | PROGRAM ELEMENT NO. | PROJECT NO. | TASK NO | WORK UNIT ACCESSION NO. |
| AFGL/PHK HANSCOM AFB, MA 01731 | 62101F | 7661 | 12 | AJ |

**11. TITLE (Include Security Classification)**
A Projectile Probe for Measuring the Electric Field Inside a Spacecraft Plasma Sheath (unclassified)

**12. PERSONAL AUTHOR(S)**
Mark N. Horenstein, Gary Freeman

| 13a. TYPE OF REPORT | 13b. TIME COVERED | 14. DATE OF REPORT (Year, Month, Day) | 15. PAGE COUNT |
|---|---|---|---|
| Final Report | FROM 2/14/84 TO 3/3/87 | 87-Mar-3 | 76 |

**16. SUPPLEMENTARY NOTATION**

| 17. | COSATI CODES | | 18. SUBJECT TERMS (Continue on reverse if necessary and identify by block number) |
|---|---|---|---|
| FIELD | GROUP | SUB-GROUP | electric field measurements, plasma, sheath, sensors |
| | | | probe, surface charge, sphere, projectile, floating |

**19. ABSTRACT (Continue on reverse if necessary and identify by block number)**

A self contained electrically floating spherical electric field probe has been developed use in volume regions where spatial field variation occurs on a length scale larger than the sphere diameter. In plasma sheath, the sphere floats to the local plasma potential, minimizing field perturbation, and provides a value of field magnitude found from the Laplacian spherical harmonic field solution. The sphere is also capable of monitoring the amount of charge collected on its own surface--a quantity that can in principle be used to infer properties of the ambient plasma.

The 15 cm battery operated aluminum sphere contains six miniature 800 Hz field mill sensors, a synchronous detection data acquisition system and A/D converter, and and 50 MHz digital fm transmitter. Data is sent at 1200 BAUD to a nearby receiver and computer for processing in real time. Fields as low as 50 V/m can be detected with a sampling time of about 1 second. At present the probe works well in air and vacuum, but has been only partially successful in plasma.

| 20. DISTRIBUTION/AVAILABILITY OF ABSTRACT | 21 ABSTRACT SECURITY CLASSIFICATION |
|---|---|
| ☒ UNCLASSIFIED/UNLIMITED ☐ SAME AS RPT. ☐ DTIC USERS | unclassified |

| 22a. NAME OF RESPONSIBLE INDIVIDUAL | 22b TELEPHONE (Include Area Code) | 22c OFFICE SYMBOL |
|---|---|---|
| George Murphy | | AFGL/PHA |

DD FORM 1473, 84 MAR     83 APR edition may be used until exhausted     SECURITY CLASSIFICATION OF THIS PAGE
All other editions are obsolete

UNCLASSIFIED

# 1. SUMMARY:

A completely self contained, electrically floating, spherical electric field probe has been developed for measuring dc electric field magnitudes in volume regions where the spatial field variation occurs on a length scale larger than the sphere diameter. In plasma sheath, the sphere floats to the local plasma potential, and thus minimizes perturbation of the field existing in its absence. The field is inferred by solution of the Laplacian spherical harmonic field equations, and thus provides a means to unambiguously measure volume fields. The sphere is also capable of monitoring the amount of charge collected on its own surface--a quantity that can in principle be used to infer the properties of the ambient plasma sheath using the theory of spherical Langmuir probes.

The 15 cm diameter aluminum sphere contains six miniature 800 Hz field mill sensors, a synchronous detection data acquisition system and A/D converter, a digital fm transmitter operating at 50 MHz, and batteries. It sends data at 1200 BAUD to a nearby receiver and computer for real time interpretation and processing. The probe is capable of measuring fields as low as 50 V/m, with a time constant of about 1 second, and operates for several hours on one set of batteries.

In its present configuration, the probe works well in air and vacuum, but has been only partially successful in plasma.

| Accession For | |
|---|---|
| NTIS GRA&I | ☒ |
| DTIC TAB | ☐ |
| Unannounced | ☐ |
| Justification | |
| By | |
| Distribution/ | |
| Availability Codes | |
| Dist | Avail and/or Special |
| A-1 | |

DTIC
COPY
INSPECTED
6

## 2. PREFACE:

The purpose of the work performed under this AFGL contract was to develop a laboratory prototype of a spherical electric field probe that ultimately could be ejected from or tethered to a space vehicle, and used to measure the dc electric field inside the surrounding plasma sheath. The basic concept of a surface field sensor incorporating a vibrating reed element was previously investigated under Grant ECS-81-06475 from the National Science Foundation. Under this AFGL contract, the sensor on the sphere were modified for use in plasma and upgraded to detect the low electric field magnitudes typical of the space environment.

The results of this investigation have been encouraging, in that a working prototype capable of measuring electric fields in air and vacuum has been developed and tested. In addition, some measurements were obtained in plasma, but not with complete success. At the present time, the difficulty appears to be a problem in the design of the surface field sensors which are contained within the spherical probe. When exposed to plasma, these sensors exhibit a significant dc drift as plasma ions flow into the apertures on the sphere surface. This problems appears to be a solvable one, however, and ultimately should not prevent the spherical probe from being a useful measuring tool.

Table of Contents

## 3. INTRODUCTION:

The interaction of both high and low altitude orbiting spacecraft with ambient plasma, and the resulting phenomena of spacecraft charging, are problems that have been well studied and investigated [12,13]. Considerable interest has focused on the structure and extent of the plasma sheath that surrounds the space shuttle and other orbiting craft, particularly in the wake region [14]. As an aid in the study of this phenomena, it would be useful to obtain measurements of both the electric field strength and the plasma parameters in the sheath region, and to do so without disturbing the character of the plasma itself.

Obtaining electric field measurements in volume regions has always been an elusive task, and one subject to much compromise and lack of accuracy. The problem arises because to date all instruments designed to measure volume fields have had to rely on a supporting arm or cable to both enter the volume region and to provide a transmission medium to bring the data signal from probe to recording instrument. The problem is particularly difficult in a plasma, because the presence of space charge further adds to the distortion of the electric field as ions collect on or flow to the supporting structure.

Investigators who have attempted volume field measurements in air have chosen probes with near spherical symmetry, because a sphere distorts an otherwise uniform field in a precisely known way. One experiment [1] used a small split sphere to monitor ac fields via the induced current between hemispheres. The conducting support rod, which also carried the signal wires, had to be located on an equipotential of the field system, so as not to greatly perturb the field from the known spherically distorted case. In another experiment [2], a rotating field mill sensor was embedded inside a conducting electrode held atop an insulating rod, together with a self contained, battery operated data acquisition system which sent its signal to ground over a nonconducting fiber optic cable. Other experimenters [3,4] have also utilized the fiber optic cable isolation principle. In this case, the presence of the support rod and fiber optic cable, though both insulating, still introduced a dielectric (i.e. capacitive) perturbation to the field. Moreover, the small but

1

still finite conductance of the "insulating" rod could in time force the spherical probe to ground potential under dc conditions, thereby diminishing the effect of its dielectric isolation. Still other researchers [5] have used a combination of both techniques in the presence of field and ions by covering a conducting support rod with a dielectric outer covering.

The ability to develop a probe capable of measurements in air does not necessarily guarantee an instrument that will function in plasma. As Fahleson [15] points out in his review of ionospheric work, electric field measurement techniques utilizing surface field sensors "work perfectly well in a uniform atmosphere, but when immersed in a plasma serious difficulties appear. One of these is that the field mill will be covered by a plasma sheath that may change the field strength at the surface by orders of magnitude". The success of surface field probe techniques in a plasma environment thus requires that reliable correction factors to field mill sensor readings be obtained, based on independently measured conditions within the plasma and on theoretical calculations. In our experiments in the lab, for example, the properties of the plasma sheath field were estimated using simple one-dimensional plasma sheath models, and compared to probe measurements using the theory of spherical Langmuir probes.

As will be discussed in Section 6.7, correlation between theory and experiment was hampered somewhat by a sensor saturation effect, which occurred with varying severity in different types of plasma. In the work reported in Section 6.8, this saturation effect was successfully modelled and correlated to actual measurements in plasma. Because the model for the saturation effect predicts actual sensor behavior with surprising accuracy, it is hoped that a revised sensor can be developed that will eliminate the saturation problem.

2

## 4. THEORY OF OPERATION:

**4.1 Space Charge Free Case (Measurements in Air):**
If an isolated conducting sphere is placed in an otherwise uniform electric field, the resulting field pattern, and in particular the field incident on the surface of the sphere, can be computed in closed form from Laplace's equation. The problem is a classical one, known to every student of elementary field theory. In specific, in the coordinate system of Fig 1, the field in the neighborhood of the sphere is given by: [6]

$$E_r = E_o \cos\theta \ \left[ \ 2\left( \frac{R_s}{r} \right)^3 + 1 \ \right] \qquad (1)$$

$$E_\theta = E_o \sin\theta \ \left[ \ \left( \frac{R_s}{r} \right)^3 - 1 \ \right] \qquad (2)$$

where $E_o$ is the uniform ambient field that exists without the sphere present, $R_s$ is the radius of the sphere, and $\theta$ is the angle measured relative to the ambient field direction.

The field incident on the surface of the sphere at radius $R_s$ is obtained by substituting $r=R_s$ into Eqn (1), to yield:

$$E(R_s) = 3 \ E_o \cos\theta \qquad (3)$$

Although the volume field loses its uniformity with the sphere present, the distortion takes place in a precisely known way, so that knowledge of the field magnitude at any known angle $\theta$ on the surface of the sphere leads directly, via Eqn(3), to a knowledge of the ambient field $E_o$ that existed before the sphere was present. If the ambient field is not everywhere uniform, the solutions (1) and (2) are still valid to within 5% if the field is almost uniform over a space of about two sphere radii. Hence the expressions (1) and (2) can be used to represent a field that is slowly varying in space.

In principal, it is possible to construct a probe from such a sphere by simply imbedding a surface field sensor at some known angle $\theta$ to the
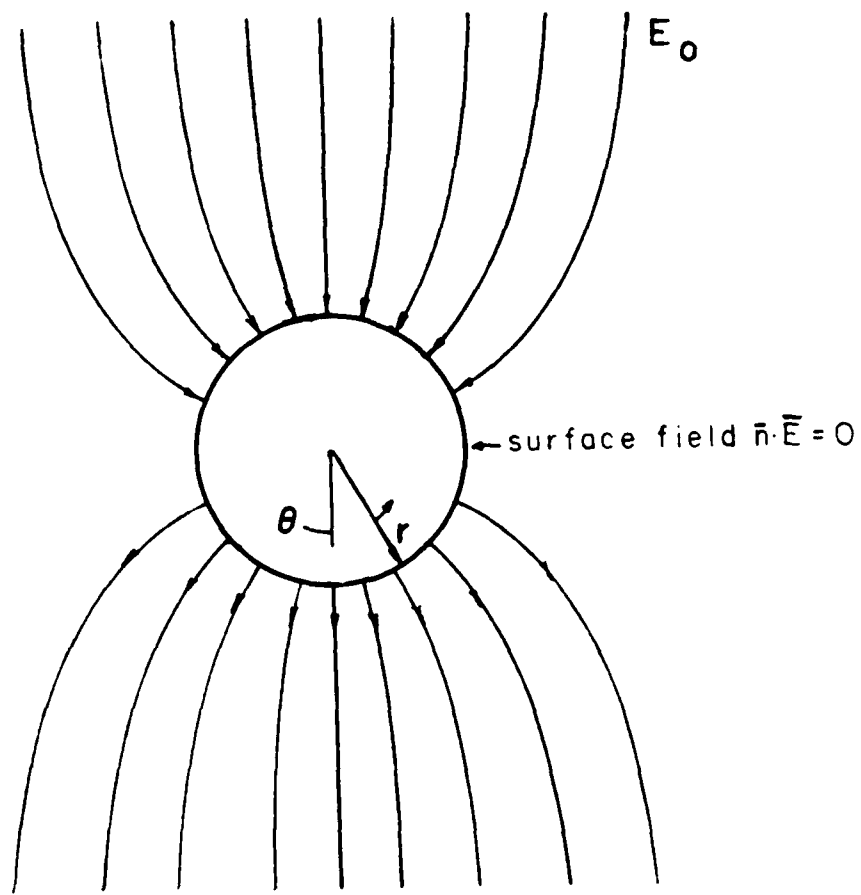
3

Figure 1 - Field pattern and coordinate geometry system for a conducting sphere in an otherwise uniform electric field, as given by Eqns (1) and (2).

field direction, and monitoring its output. As a practical matter, if a
spherical probe is ejected without mechanical supports into a volume field
region, control, or even knowledge, of the angle $\theta$ is not possible. This
problem can be overcome by sampling the surface field magnitude at three
points, each lying on an end of one of the three orthogonal axes of the
sphere, as shown in Fig 2. If the polar z-axis of the sphere's coordinate
system is inclined at an arbitrary angle $\phi$ to the ambient field direction,
and the sphere's x-axis is rotated at an angle $\alpha$ relative to the plane of
the z-axis and the field direction, the resulting surface field
components, measured at the ends of the three orthogonal X, Y, and Z axes,
are given by:

$$X\text{-axis:} \qquad E_X = 3E_o \sin \phi \cos \alpha$$

$$Y\text{-axis:} \qquad E_Y = 3E_o \sin \phi \sin \alpha$$

$$Z\text{-axis:} \qquad E_Z = 3E_o \cos \phi \tag{4}$$

The magnitude $E_o$ of the ambient field can be determined from these X,
Y, and Z axis surface measurements by taking the square root of the sum of
squares, i.e.:

$$[E_X^2 + E_Y^2 + E_Z^2]^{1/2} = 3E_o \ (\sin^2\phi\cos^2\alpha + \sin^2\phi\sin^2\alpha + \cos^2\phi)$$

$$= 3E_o \tag{5}$$

Note that the orientation angles $\phi$ and $\alpha$ do not appear in Eqn (5),
indicating that the field measurement can be obtained regardless of
orientation of the sphere relative to the ambient field direction. The
trade-off involved in the orthogonal axis sampling scheme is the loss of
information about the vector direction of the ambient electric field,
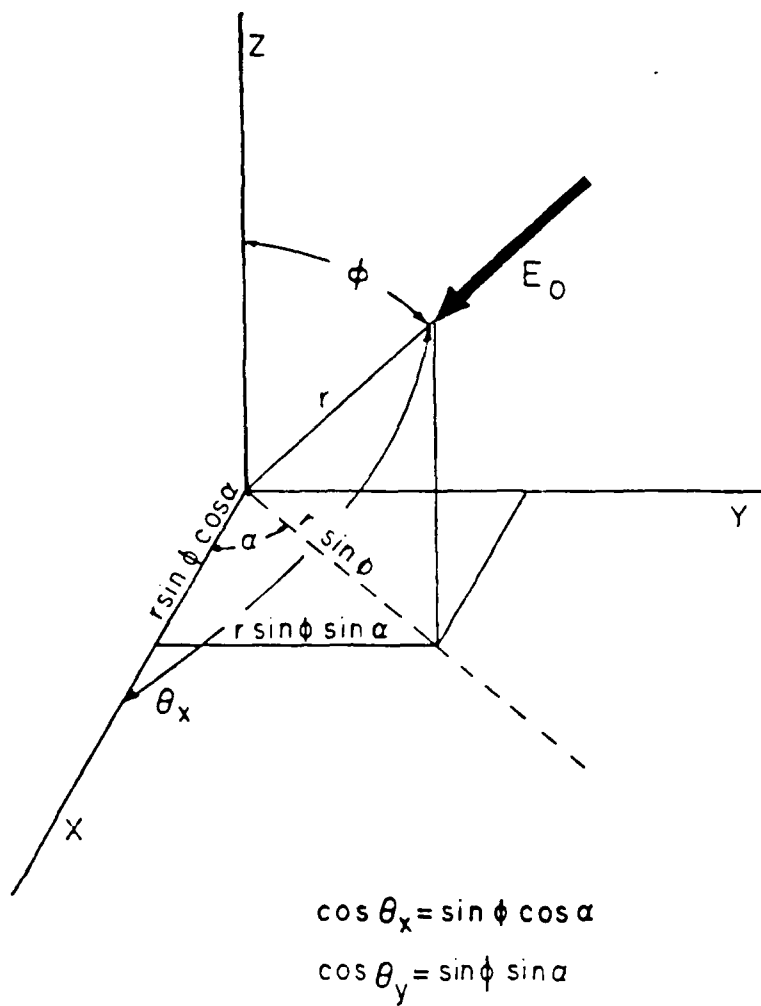since Eqn (5) yields just its magnitude.

$$\cos \theta_x = \sin \phi \cos \alpha$$

$$\cos \theta_y = \sin \phi \sin \alpha$$

Figure 2 - Coordinate system used in the derivation of Eqns (4) and (5,. The angle between the sphere's polar ("z") axis and the ambient field direction is $\phi$, while $\alpha$ is the angle between the x-axis and the projection onto the x-y plane of the z-$E_0$ plane.

6

## 4.2 Theory With Space Charge Present

In a plasma, ions will impact on the spherical probe, causing it to acquire a net charge which increases until the probe has reached the floating plasma potential. This charging mechanism has been the subject of considerable theoretical and experimental investigation, and is discussed in more detail in Section 8. In this section, we discuss the ability of the spherical field probe to measure the magnitude of the collected charge.

Charge that does collect on the probe because of the presence of plasma will distribute itself uniformly around the equipotential surface of the sphere, so that a uniform radial field component will be superimposed on the spherical harmonic radial field solution (1). This extra radial field component will be equal to:

$$E_Q = \frac{Q}{4\pi\epsilon_o R_s^2} \qquad (7)$$

and the resulting total field pattern will look something like that of Fig 3, which depicts the sphere with an arbitrary amount of positive collected charge. Despite the seemingly asymmetric distortion of the electric field, it is nevertheless composed of the odd-symmetric ambient field solution (1) and (2), and the radially symmetric collected charge field solution (7). These two field components can be separately measured on the probe by sampling the sphere's radial surface field at six, rather than three sampling points, each located on one end of the sphere's orthogonal coordinate axes. A *differential* measurement between any two sensors on a given axis will cancel the $E_Q$ component, leaving only the $E_o$ component, while a *common mode* measurement between two sensors on a given axis will cancel the $E_o$ component, leaving only the $E_Q$ component. Thus, for a given set of surface field measurements $E_X$, $E_X'$, $E_Y$, $E_Y'$, $E_Z$, and $E_Z'$, taken at six orthogonal axes sampling points, the ambient field magnitude $E_o$ and collected charge $Q$ are given by:
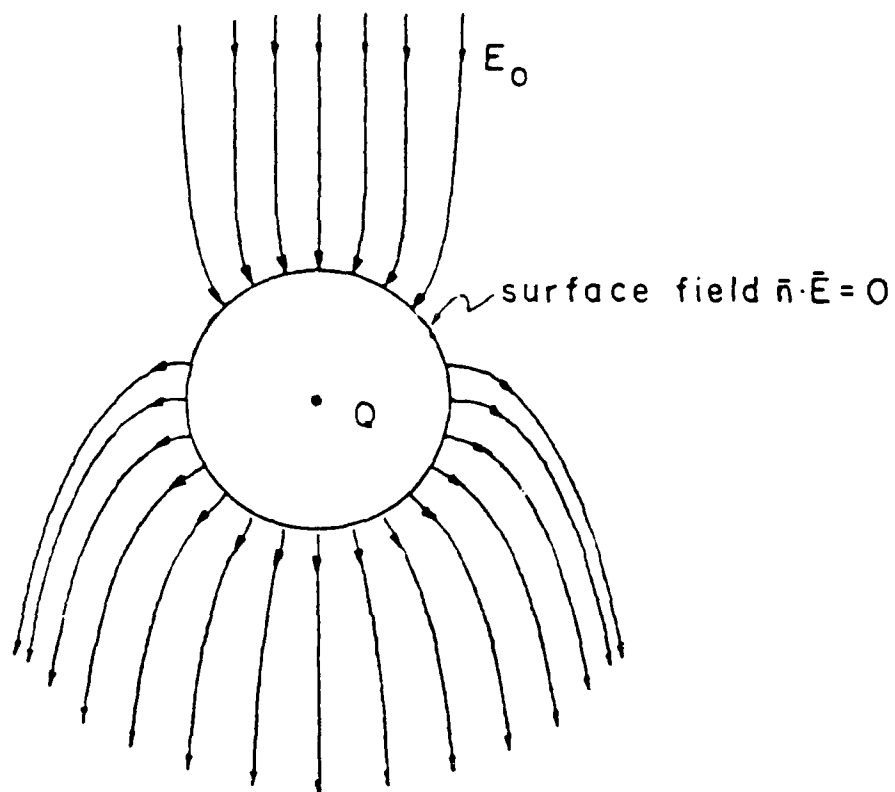
7

Figure 3 - Field pattern for a conducting sphere in an otherwise uniform electric field when the sphere also has charge collected on its surface, as given by Eqns (1), (2) and (7). Shown here is an arbitrary amount of positive collected charge less than $Q_{sat}$.

$$E_o = \frac{1}{6} \; [ \; (E_X - E_{X'})^2 + (E_Y - E_{Y'})^2 + (E_Z - E_{Z'})^2 \; ]^{1/2} \qquad (8)$$

$$Q = \frac{1}{6} \; [ \; (E_X + E_{X'}) + (E_Y + E_{Y'}) + (E_Z + E_{Z'}) \; ] \cdot \quad 4\pi\epsilon_o R_s^2 \qquad (9)$$

where the primed quantities indicate the three extra "opposite-end" surface field measurements, and where Eqns (5) and (7) have been utilized.

Once the collected charge Q is known, it can in principle be combined with the plasma charging theories outlined in Section 8 to obtain information about the properties of the ambient plasma in the vicinity of the sphere.

## 5. INSTRUMENTATION

The ideas presented in the preceding sections have been incorporated into a working probe, built inside a six inch diameter spherical aluminum shell. The the functional block diagram of the instrument is shown in Fig 4, while a sketch of its basic layout is shown in Fig 5. The surface field sensors consist of miniature, individually calibrated tuning fork electric field mills operating at 800 Hz, with a field sensitivity as low as 100 V/m. Each field mill at is present interfaced to a 1 Hz bandwidth synchronous detector, although faster synchronous detection is possible at the expense of reduced instrument sensitivity. Conversely, enhanced sensitivity is achievable with smaller bandwidth synchronous detection. The six synchronous detector outputs are fed to a microprocessor controlled data acquisition system, whose digital output drives an fm frequency-shift-keyed, amplitude modulated carrier (fsk-am) 1200 baud radio transmitter and antenna. Although the antenna structure shown in Fig 5 upsets slightly the spherical symmetry of the probe, the perturbation is minor, and does not affect the field signals seen by each of the six surface sensors. The receiving section consists of a phase-locked loop receiver, digital decoder, and host computer, which collects and processes the raw sensor data and performs the needed calculations (8) and (9) before data is displayed or recorded.

To be useful, the collected field data must be coordinated with the position at which the data is taken. If the position vs. time characteristic of the probe is known, i.e. if the probe is sent on a known ballistic trajectory through a given sheath region, then the time at which data is received can be used to determine the position at which it was obtained. Thus for each data point, the probe transmits a "time-mark" code word at the precise instant that all six sensors are simultaneously interrogated. Errors caused by the finite time lapse needed to serially transmit the data from the six sensors are thus avoided. At the end of each data point sequence, the probe also transmits a coded "status word", which indicates that all systems inside the sphere are functioning normally.

A summary of probe specifications and characteristics is given in Table I. Details of the various component modules of the probe, including component layouts and circuit schematics, are included in Appendix B.
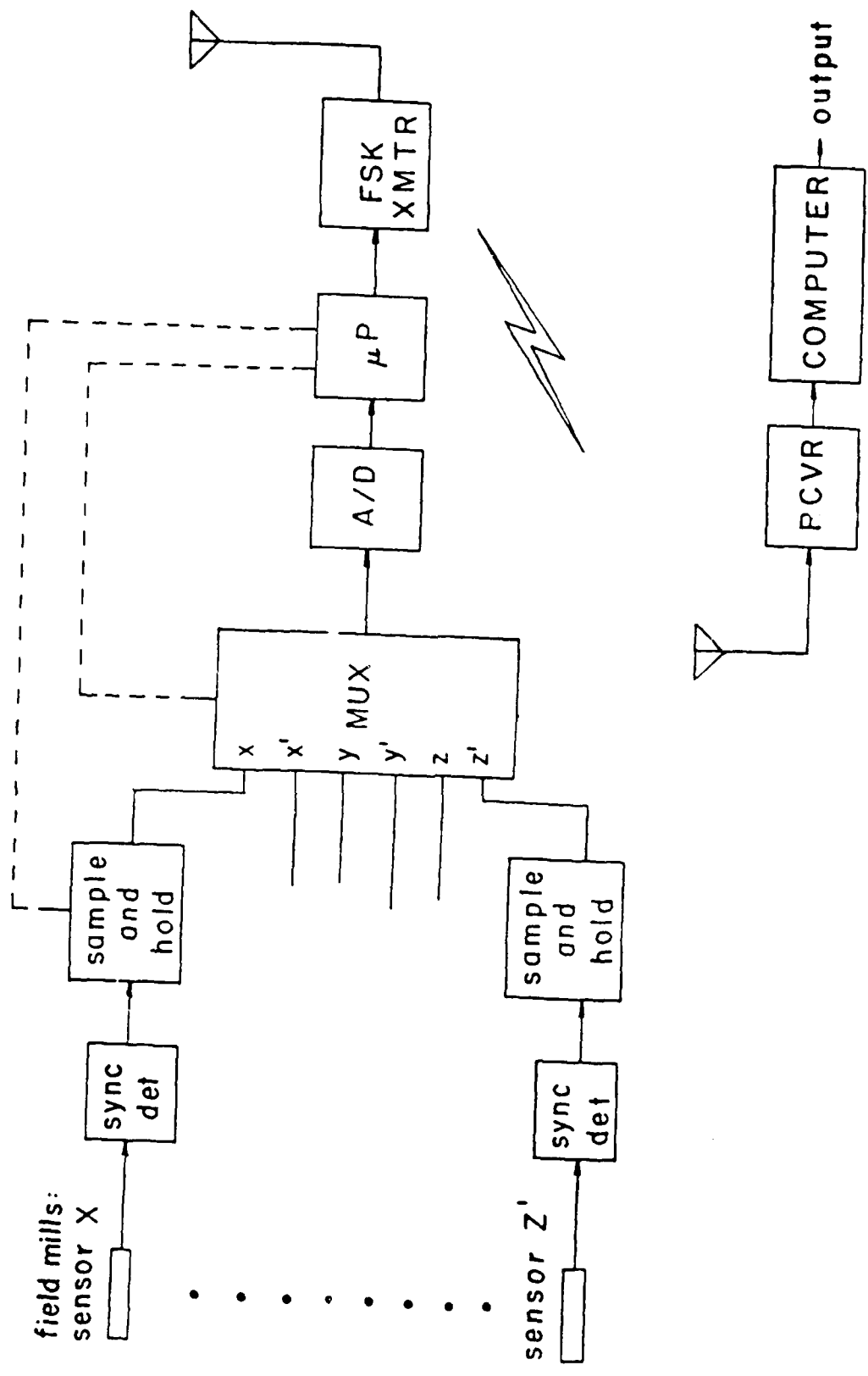
10

Figure 4 – Functional block diagram of the spherical probe system, showing sensors, data acquisition components, transmitter, receiver, and data processing computer.
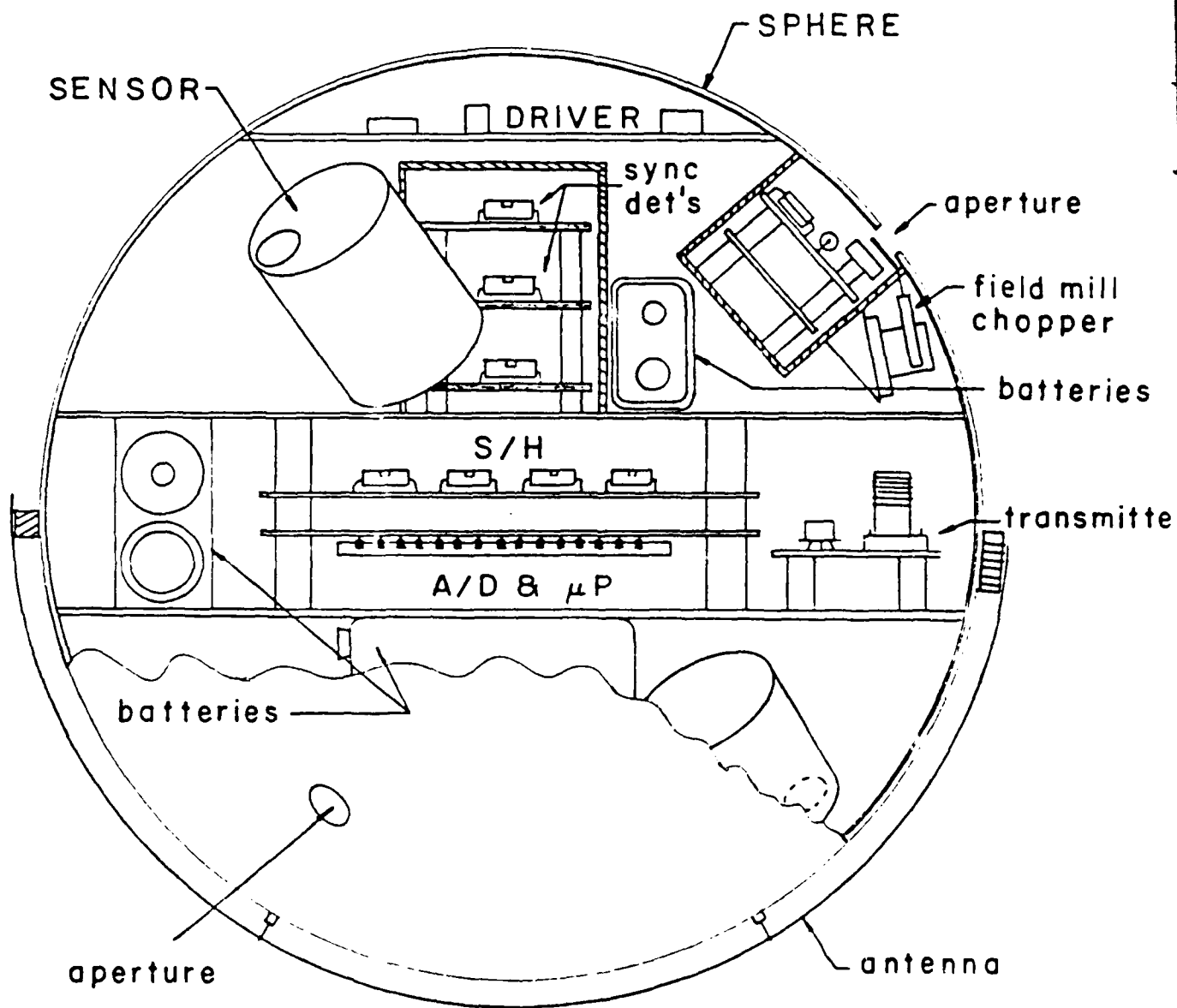
Figure 5 - Cutaway view of the spherical probe.  Not all sensors batteries are shown.

Table I - Summary of Probe Specification and Characteristics

PHYSICAL:

| | |
|---|---|
| Sphere Diameter: | 6 in.    (15.2 cm) |
| Sphere Weight: | 2.5 lbs (6 kg) |

ELECTRICAL:

| | |
|---|---|
| Power Consumption: | $\simeq$1.7 Watts (probe only) |
| Battery Requirements: | 6 @ 7.0 V min ("9V battery") |
| | 4 @ 1.2 V min ("AAA cell") |

SENSORS:

| | |
|---|---|
| Field Mill Chopper Freq: | 800 Hz |
| Chopper Excursion: | 1 mm |
| Sensing Aperture: | 4 mm dia |
| Field Resolution: | 50 V/m |
| Maximum Scale Reading: | 2 kV/m |
| Sensor Stability: | 1 bit per 256 (1%) |
| Sync. Detector Time Constant: | 1 sec |

DATA LINK:

| | |
|---|---|
| FM Transmitter Frequency: | 49 MHz |
| Data Transmission Rate: | 1200 baud |
| Probe Antenna Configuration: | tuned open strip wire |

# 6. TESTS RESULTS

## 6.1 Test Results in Vacuum Without Plasma

Physical and electrical floating probe conditions are difficult to
simulate in the gravity environment of the lab, because the transit time
of a free falling body is quite short. An approximate test procedure was
used as a means of testing the theory of probe operation in plasma. The
spherical probe was hung by a fine nylon thread between parallel plate
uniform field producing electrodes in a manner that simulated, to the
maximum degree possible, true electrically floating probe conditions. The
thread does distort the field a little, and over time does conduct charge
to the sphere. Nevertheless, the thread-hanging test procedure was used
because it allowed the various field and charge measuring systems and
algorithms to be functionally tested, as will be described shortly. The
field distortion problem was minimized by always situating the thread on a
known equipotential of the field system, i.e. parallel to the plate
electrodes and perpendicular to the sphere's equator, and by attaching the
thread to the sphere at a point far removed from the surface sensors. The
charging of the sphere by the finite conductivity of the thread, which is
caused by surface moisture collected on the thread, is not easy to
eliminate in air--however in vacuum the thread surface conductivity
becomes very small. In addition, because the thread is so thin, the
effects of plasma interaction are minimal.

As a side note, when tests were performed in air, the charging time
constant of the thread-probe system could actually be monitored from the
increase of the $E_Q$ component over time. Since, in principle, the probe
capacitance can be estimated, the resistance of the thread can also be
found.

Fig 6 shows the sphere's $E_O$ output in V/m as a function of both
positive and negative actual ambient fields, with the sphere held at a
constant orientation angle to the field. As expected, the relationship is
a linear one. Note that positive and negative applied fields both yield
positive sphere output, because the probe measures just the magnitude of
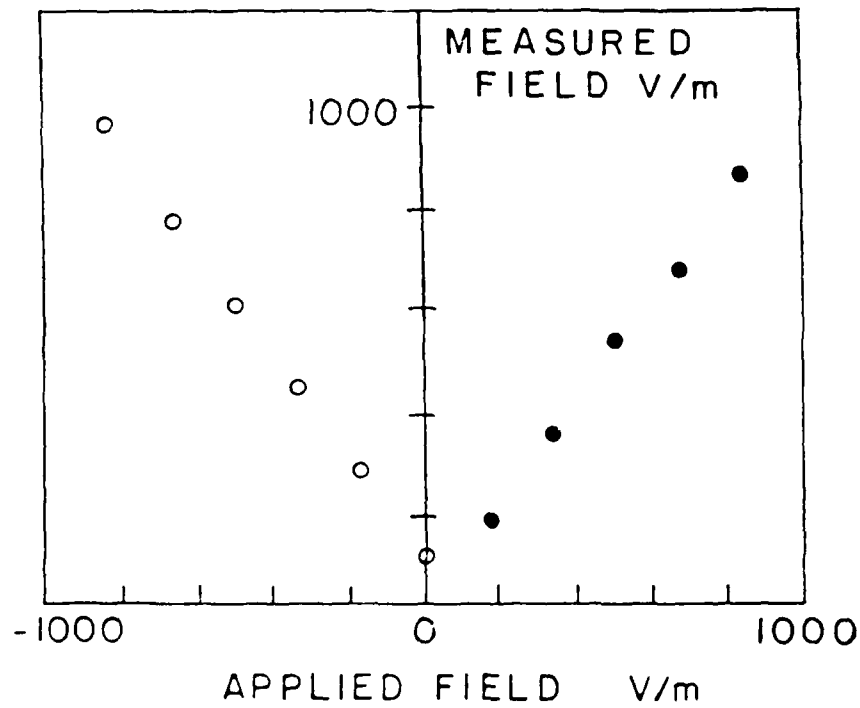
14

Figure 6 - Measured ambient field versus applied ambient field, with the sphere held at constant angle relative to the ambient field direction. Since the probe provides a measure of field magnitude only, the output is positive for both polarities of applied ambient field.
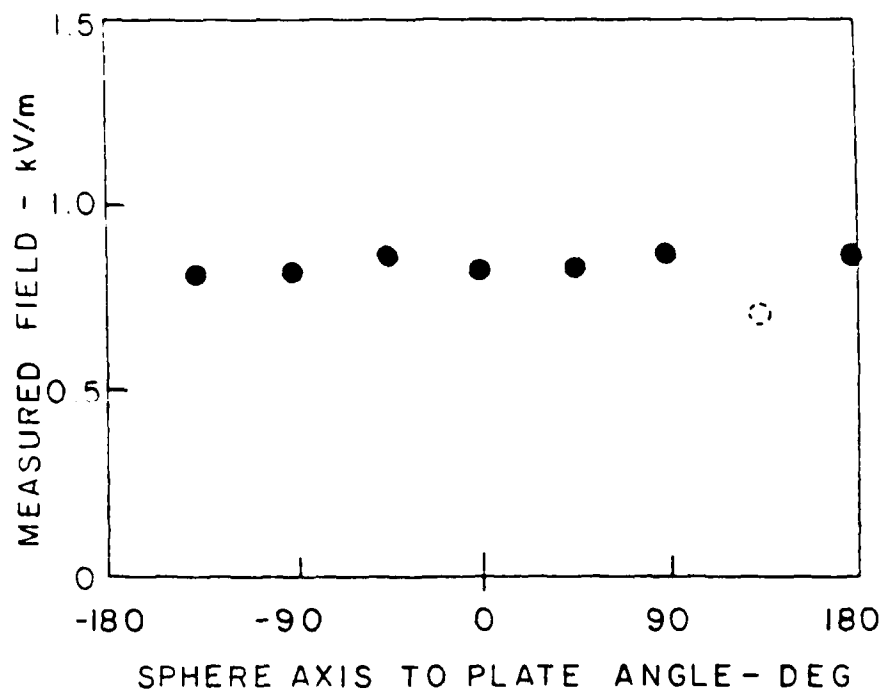
Figure 7 - Output of the probe at constant ambient field of 800 V/m, with the sphere held at different angles relative to the ambient field direction.

the ambient field. Figure 7 shows the ambient field component $E_o$ measured with the sphere's polar axis oriented at various angles to the ambient field direction for a constant ambient field magnitude of 800 V/m. Again, as predicted by Eqn (5), the measurement is independent of angle.

The ability of the probe to measure its own collected charge was tested using the experimental configuration of Fig 8, in which the probe was *grounded* by a fine thread, again situated as much as possible along an equipotential of the electrode system. The parallel plates, located at distances $d_1$ and $d_2$ from the sphere center, were energized to different voltages $V_1$ and $V_2$ relative to ground. An analysis of this electrode system [5,6] shows that if the field distortion caused by the wire is neglected, the potential and field solutions at the surface of the sphere are given, for the case $d_1=d_2=d$, by:

$$\phi = 0 \tag{10}$$

and

$$E_r = 3 \ E_o \ \cos\theta \ + \ \frac{(V_1+V_2)}{2} \cdot \frac{1}{R_s} \tag{11}$$

where

$$E_o = \frac{V_1-V_2}{2d} \tag{12}$$

The second field component in (11) is a byproduct of the "floating" potential that would exist between the plates at the sphere's center in the absence of the sphere. Note that this field component is independent of angle around the sphere. It can thus be used to simulate the collection by the sphere of a net charge Q. The values of the simulated charge Q and field $E_Q$ are given, in terms of the imbalance between the voltages $V_1$ and $V_2$, by:
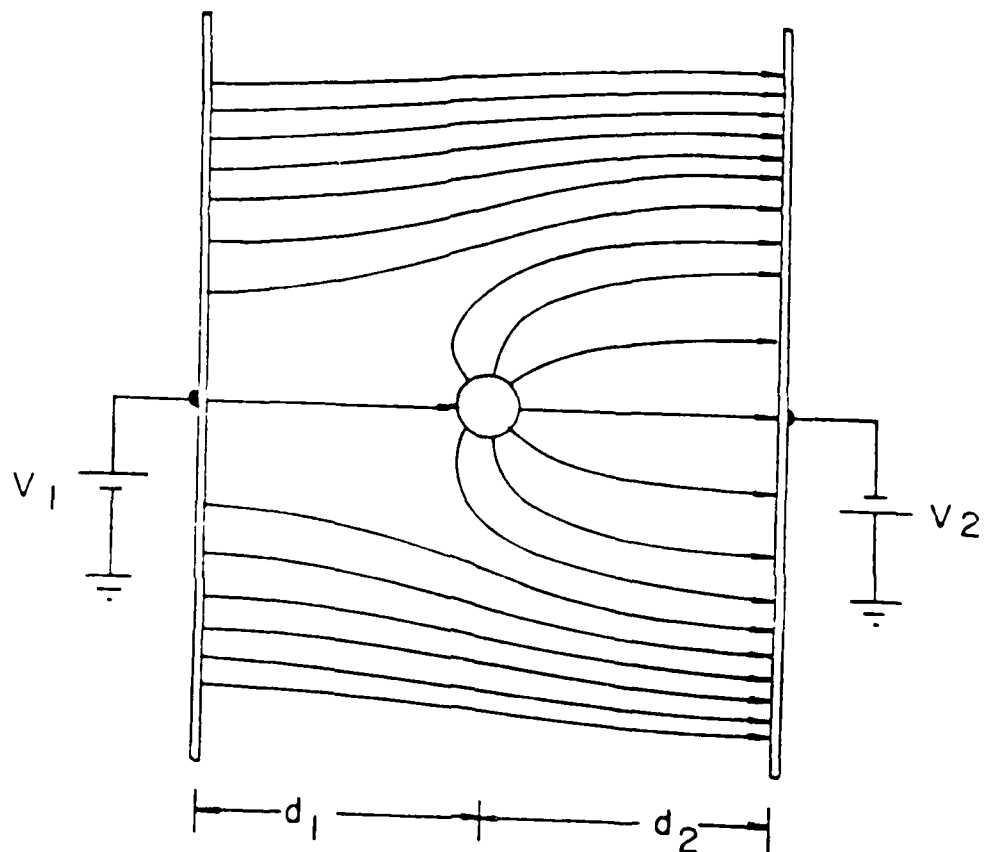
Figure 8 - Configuration and resulting field pattern used to simulate the sphere with a known amount of collected charge. Surface field component is given by Eqns (11) and (12)

$$Q = 4\pi\epsilon_o R_s \cdot \frac{(V_1 + V_2)}{2} \tag{13}$$

$$E_Q = \frac{Q}{4\pi\epsilon_o R_s^2} = \frac{V_1 + V_2}{2} \cdot \frac{1}{R_s} \tag{14}$$

Note that Q in fact does represent the net charge induced on the sphere in the configuration of Fig 8. The value of $E_Q$, the radial surface field associated with this "simulated" Q, is given by the second term in Eqn (11).

A plot of the measured $E_Q$ component as a function of the simulated $E_Q$ component, calculated from Eqn (14) for various voltages $V_1$ and $V_2$, is shown in Fig 9, together with the simultaneously measured $E_o$ component given by Eqn (12). The plot shows that the probe is indeed capable of measuring its own collected charge while simultaneously measuring the value of the local ambient field.
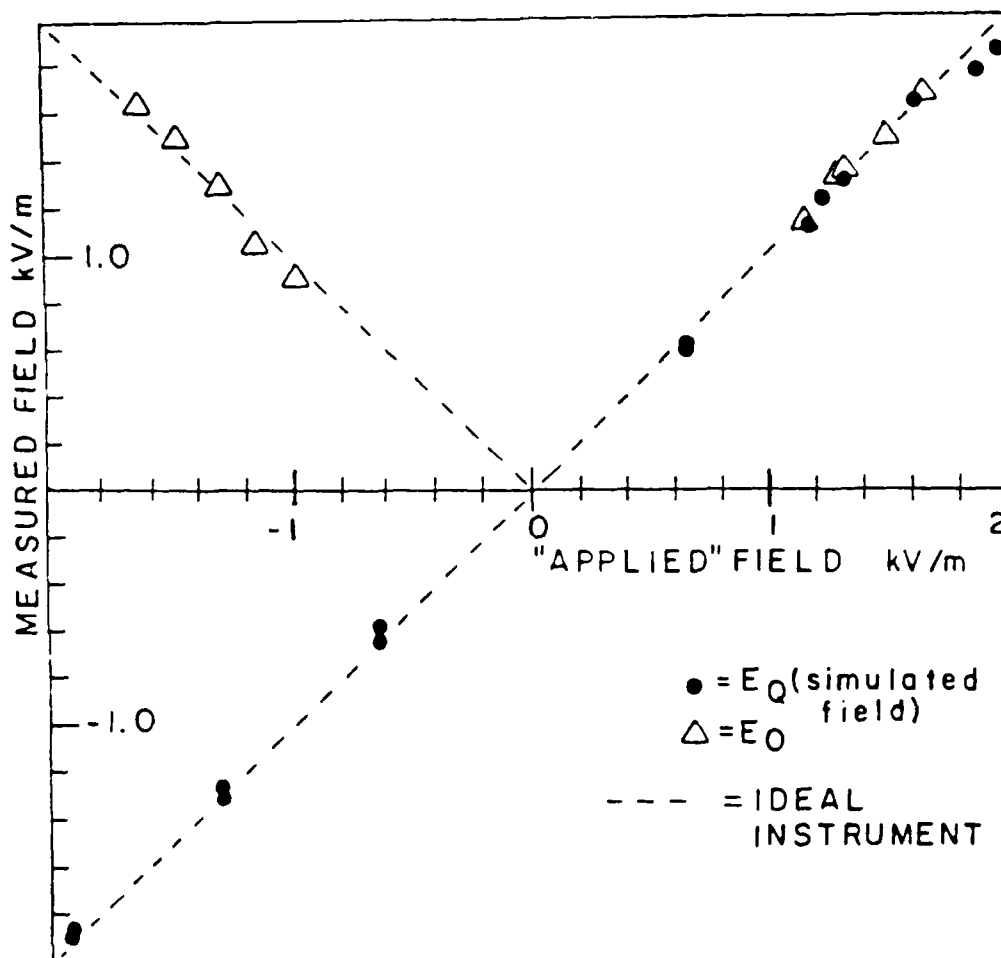
Figure 9 - Measured ambient field and collected charge field components vs. applied ambient field, for the configuration of Figure 8, with $d_1 = d_2$. The actual ambient, and the actual simulated collected charge fields, i.e the output of an ideal instrument, are noted by the dotted lines.

## 6.2 Plasma Modelling and Measurements Without Probe

The characteristics of the plasma without the probe present were
investigated as a means of evaluating subsequent probe measurements.  The
first step in the development of a model for the plasma is an
understanding of the dominant plasma properties in the test chamber.  In
our case, the key processes are steady state, and involve low density,
partially ionized Argon gas.  In order that the behavior of the probe be
evaluated, key scalar parameters such as density and temperature are
required for use in numerical simulations of the plasma sheath field.  To
measure these parameters, conventional Langmuir probe tests were
performed, with the chosen plasma chamber that of parallel plate geometry,
so that the plasma sheath problem could be reduced to the one dimensional
case.  As will be shown, the critical factors for the sheath simulation
are the proper choice of the ion and electron distributions as a function
of applied plate voltage.

The fundamental property of a plasma is its ability to shield out
electric potentials applied to it.  If a given potential $\phi$ is applied to
an electrode in a plasma, charge of the opposite sign will collect around
the electrode.  Thermal motions of the charged particles will cause the
charge cloud surrounding the electrode to be of a finite thickness on the
order of the Debye length.  The standard derivation of the Debye length
commonly uses a zero ion temperature limit approximation that is valid for
a low density plasma.  This approximation assumes the ion-electron mass
ratio to be so large that the inertia of the ions keeps them in relatively
fixed positions relative to the moving electrons.  This mass ratio
information can be related to temperature by examining the case where
there is complete momentum transfer for electron-ion collisions, i.e.:

$$m v_e = M v_i$$

or

$$v_i = \frac{m_e}{M_i} v_e$$

21

In these equations, $m_e$ and $v_e$ are the electron mass and velocity, and $M_i$ and $v_i$ are the ion mass and velocity.

The ion temperature is given by:

$$T_i = \frac{M_i v_i^2}{3k} = \frac{m_e}{M_i} T_e$$

Thus, for the condition $M_i/m_e \gg 1$, it will be true that $T_e \gg T_i$. Using this approximation, the ion density $n_i$ can be set equal to the plasma density at infinity, i.e. to $n_o$.

A second simplifying assumption often used in low-density plasma calculations assumes the electron density distribution to be Maxwellian, with electron density given by:

$$n_e = n_o \, e^{\phi/V_t}$$

In this equation, the thermal voltage $V_t$ is equal to $kT_e/q$. Note that for the electron distribution is to be Maxwellian, the plasma must be isotropic. The assumptions described above can be combined with the one-dimensional form of Poisson's equation to yield:

$$\frac{d^2\phi}{dx^2} = \frac{-q}{\epsilon_o}(n_i - n_e) = \frac{qn_o}{\epsilon_o}[e^{\phi/V_t} - 1] \qquad (1)$$

Linearizing Eqn (1) by a Taylor series taken about the point $\phi = 0$ results in:

$$\frac{d^2\phi}{dx^2} = \frac{qn_o\phi}{\epsilon_o V_t}$$

or

$$\phi(x) = \phi_o \, e^{\pm x/\lambda} \qquad (2)$$

where $\lambda = [\epsilon_o V_t/qn_o]$ is the Debye length.

The potential $\phi$ falls off exponentially with the Debye length, and a sheath region forms around the electrode. In the case where the electrode is floating, so that no current flows to or from it, the electrode will become negatively charged with respect to the plasma, forming an electron sheath around it. This phenomenon occurs because the thermal velocity of the electrons is much greater than that of the ions, hence the potential drop of the sheath adjusts itself so that the total particle flux to the electrode is zero. A practical technique for electric field measurement must provide some method for "zeroing-out" this potential which forms in the absence of externally applied fields.

If the zero ion temperature approximation is used, the diffusion term of the ion current equation can be neglected. This simplification leaves only the drift term in the ion current equation. When a floating electrode attains a negative potential, however, the sheath region extends from the electrode only on the order of the Debye length; hence some other mechanism must exist by which the ions are drawn to the sheath, where they are subsequently accelerated toward the negative electrode. This mechanism can be modeled by assuming a pre-sheath region in which the fields are small compared to the main sheath, but of sufficient spatial extent to accelerate the ions to some drift velocity $v_i$ at the edge of the sheath region. Within the sheath region, conservation of energy requires that the condition:

$$\frac{mv(x)^2}{2} = \frac{mv_o^2}{2} - q\phi(x)$$

(3)

be met for a given particle species, where $v_o$ is the velocity at the electrode surface. If the electron distribution is Maxwellian, the distribution functions for the ion and electron species are, respectively:

$$f_i[v(x)] = n_o\delta\left[\left[v(x)^2 + \frac{2q\phi(x)}{M_i}\right]^{1/2} - v_o\right]$$

(4)

i.e., every ion has a constant velocity $v_o$, and

$$f_e[v(x)] = n_0 \, kT_e \, \exp \left[ \frac{-m_e}{2m_e} \, \frac{}{2kT_e} \, [v(x)^2 + 2q\phi(x)/m_e] \right] \qquad (5)$$

In Eqn (4), $\delta$ represents the Dirac delta function. These expressions can be integrated over velocity to yield expressions for the particle densities as a function of potential:

$$n_e = n_0 \, e^{\phi/V_t} \qquad (6)$$

and

$$n_i = n_0 \left[ 1 - \frac{2q\phi}{M_i v_0^2} \right] \qquad (7)$$

If these density functions are to be applied to Poisson's equation, the ion velocity $v_i$ at the sheath edge must satisfy the following inequality:

$$v_0 > \left[ \frac{kT_e}{M_i} \right]^{1/2} \qquad (8)$$

i.e., the ions must stream into the sheath with an energy greater than $kT_e/2$, and the sheath edge must have a potential of $-kT_e/2q$. This inequality is called the Bohm sheath criterion. Note that the Bohm criterion is dependent on the electron temperature only, and not on the ion temperature. This fact is important in the determination of plasma parameters.


6.3 Langmuir Probe Tests of the Plasma

The Langmuir probe method provides reasonably accurate values of the plasma parameters provided that the plasma meets certain conditions. A Langmuir probe is an electrode that is placed in the plasma and biased to various potentials with respect to the plasma. The resulting I-V plot

24

provides information about the plasma parameters. The following
assumptions must be made if Langmuir probe theory is to be valid:

1) The plasma is isotropic.

2) Mean free paths are much greater than the Debye length, i.e. the
plasma is essentially collisionless, so that "free fall" conditions
prevail.

3) The zero ion temperature approximation is valid, i.e. $T_e \gg T_i$.

4) The electron distribution is Maxwellian.

If these assumptions are valid, the plasma can be completely specified by
just two scalar parameters, the electron temperature $T_e$ and the plasma
density $n_o$.

An ideal Langmuir probe I-V curve, taken from Ref [25], is depicted
in Fig 10. The voltage $V_s$ represents the potential of the ambient plasma.
When the probe is forced to this potential, the field between the probe
and plasma becomes zero. Because $T_e \gg T_i$, however, the electrons migrate
faster to the probe, causing a positive net flux of electrons to the probe
surface (i.e., a net negative current into the probe). Note that the
abscissa in Fig 10 represents $J_e$, the current flux of electrons into the
probe. If the probe potential is increased above $V_s$ (region A in Fig 10),
more electrons are attracted to it, and a sheath region develops around
the probe. Since the flow of electrons into the sheath is governed by
their thermal migration to the outer sheath edge, the resulting electron
current levels off at a relatively constant value.

If the probe potential is forced below $V_s$ (region B in Fig 10), fewer
electrons reach the probe, and the magnitude of the probe current
decreases. If the electron distribution is Maxwellian and free-fall
conditions predominate, the curve in this region will be exponential. At
the floating potential $V_f$, i.e. the point where the probe current is zero,
the electron current becomes equal to the ion current.

Well below $V_f$ (region C in Fig 10), almost all the electrons are
repelled from the probe, and an ion sheath develops around it. Since the
flow of ions into the sheath is governed by their thermal migration to the
outer sheath edge, the resulting ion current levels off at a relatively

constant value. Given that $T_e \gg T_i$, the magnitude of this ion saturation current will be much smaller and more nearly constant than the analogous electron saturation current.
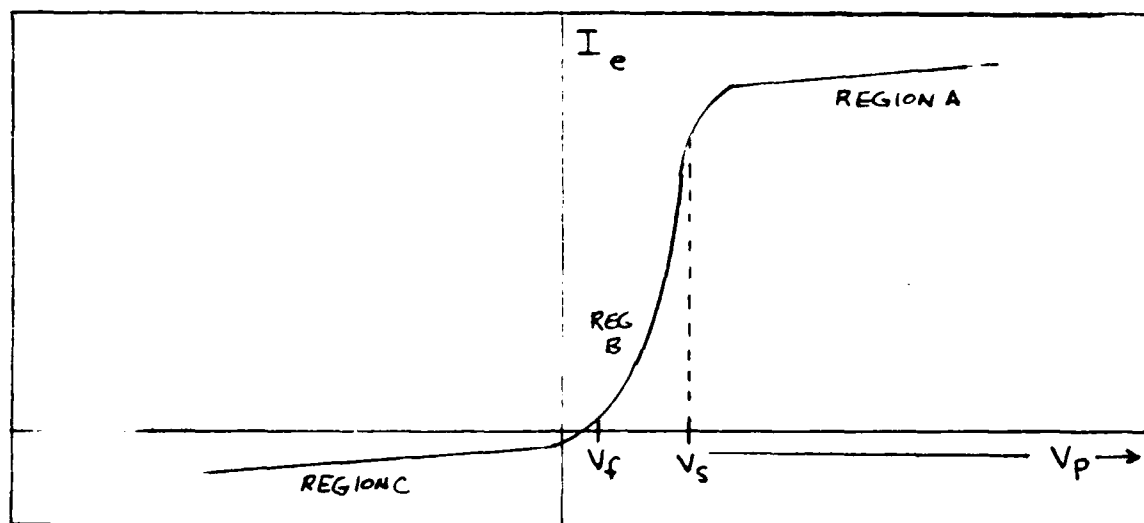


Figure 10 - Typical Langmuir Probe Curve

The traditional Langmuir probe methods described above were applied to the measured I-V characteristics of a spherical probe placed in a plasma produced in the "Jumbo" vacuum chamber at AFGL. The plasma was produced by seeding the vacuum chamber with low pressure (about 200 mTorr) background argon gas and injecting a weak (200V) electron beam toward a passive, grounded target plate. Gaseous diffusion was assumed to produce a relatively uniform plasma throughout the vacuum chamber.

The first step in the examination of the plasma parameters is the determination of the electron temperature. As noted above, the measured i-v curve is exponential in this region since the electron distribution is Maxwellian; hence the probe current is given by:

$$I = I_0 \, e^{V_p/V_t} \tag{9}$$

26

where $V_p$ is the voltage of the probe with respect to the plasma. Taking the natural log of Eqn (9) yields:

$$\ln (I) = \ln (I_0) + \frac{V_p}{V_t} \tag{10}$$

By measuring the logarithmic slope of the measured I-V characteristic in region B, the factor $1/V_t$, i.e. the inverse of the thermal voltage, can be obtained. From the Langmuir probe data obtained in our experiment,[1] the value $T_e = 9.5$ eV was found from a least squares fit of $\ln(I)$ versus $V_p$ (see Figs 11 and 12). The correlation coefficient for the logarithmic plot was 0.998, indicating that the measured curve in region B is truly exponential; likewise, the assumptions implicit in Eqns (1), (2) and (4) are verified.

Once the electron temperature is known, the plasma density $n_0$ can be determined from the ion saturation current in region C. This ion saturation current can be estimated theoretically by making use of the Bohm sheath criterion derived previously [22]. Assuming that the ions have some non-zero drift velocity obtained in the pre-sheath electric field, and assuming that the electron current can be neglected for $V_p > 3kT_e/q$, it follows that:

$$v_i = \left[ \frac{kT_e}{M_i} \right]^{1/2}$$

If the probe area is equal to A, then:

$$I = JA = qn_s v_i A = qn_s A \left[ \frac{kT_e}{M_i} \right]^{1/2} \tag{11}$$

where J and $n_s$ are the current density and particle density at the surface of the probe. Note that $n_s$ also represents the ion density at the outer

---

1[pg 120, #17 of the data notebook]

edge of the sheath region. In the derivation of the Bohm sheath criterion, the sheath edge is defined as that point at which the potential with respect to the neutral plasma is equal to $-KT_e/2q$. Assuming a Maxwell-Boltzmann distribution, it therefore follows that:

$$n_s = n_o e^{-1/2} = 0.61\ n_o$$

Substituting this expression into Eqn (11) results in:

$$I_B = 0.61\ qn_oA \left[ \frac{kT_e}{M_i} \right]^{1/2} \tag{12}$$

where $I_B$, called the Bohm current, specifies the ion saturation current flowing to the probe. Solving Eqn (12) for $n_o$, given the data shown in Fig 11, results in:

$$n_o = 1.64\ \frac{I}{qA} \left[ \frac{M_i}{kT_e} \right]^{1/2} = 4.56 \times 10^9\ /m^3 \tag{13}$$

In region C of the measured Langmuir plots of Fig 11, the current is approximately constant, indicating that Eqn (3) represents a valid assumption. Note that in region A of the plots, the current is roughly a linear function of voltage, rather than a near constant current. This effect is predicted by Langmuir probe theory for spherical probes [23].
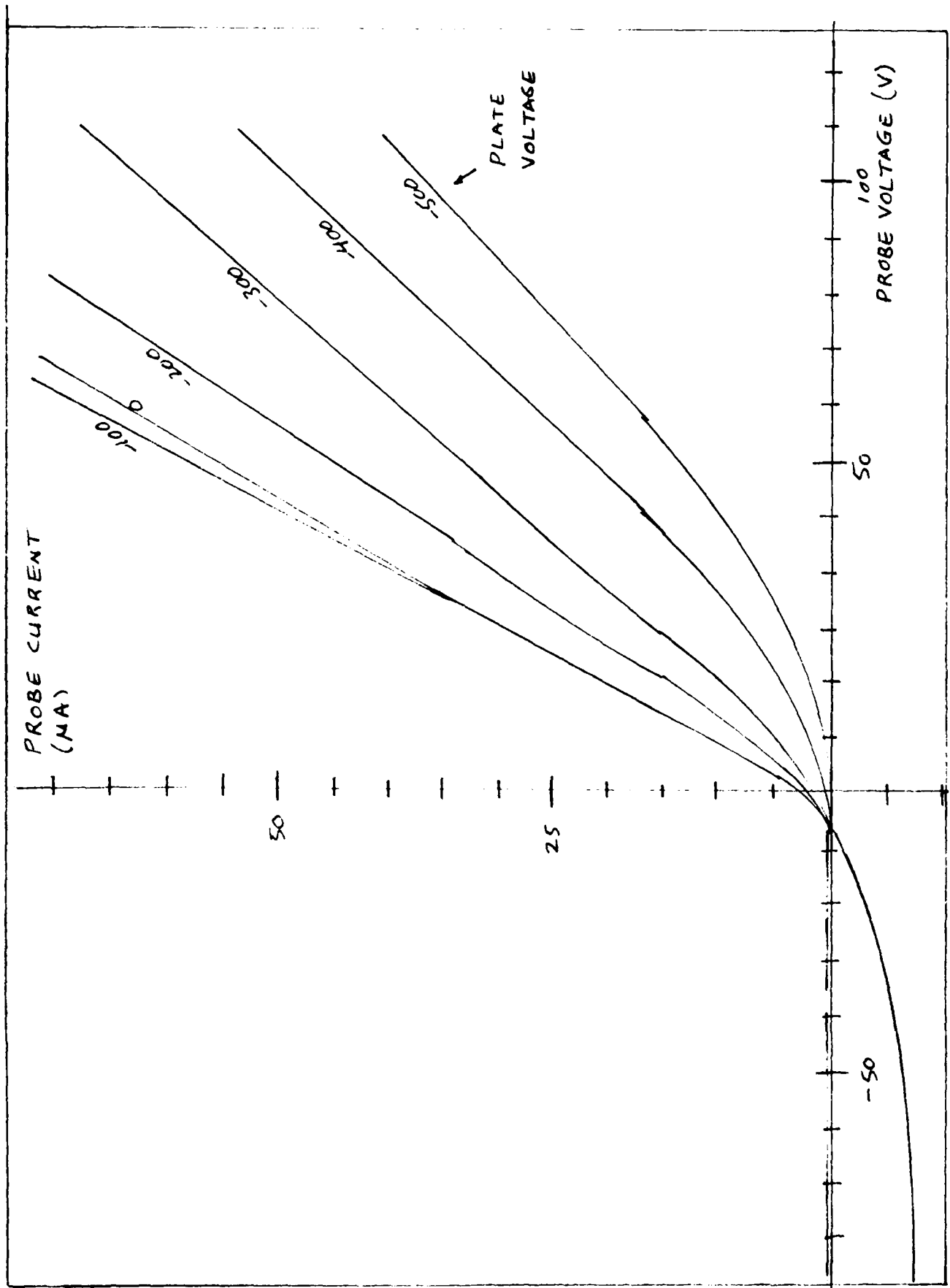
Figure 11 - Spherical Langmuir probe curves as measured in the vacuum chamber.
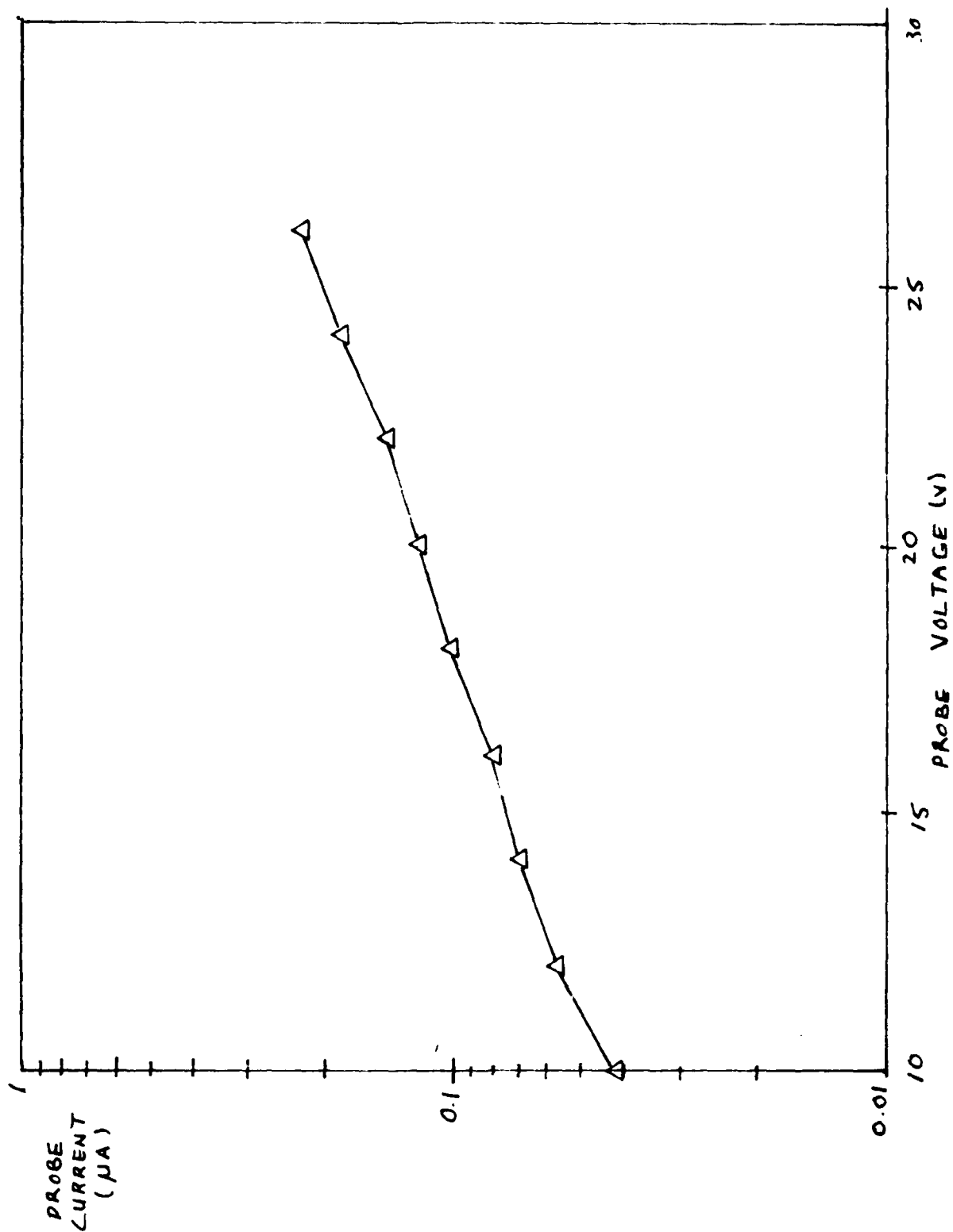
Figure 12 - Spherical Langmuir probe I-V curve plotted with a logarithmic current scale.

30

## 6.4 Electric Field Simulation Without Plasma

The plasma chamber geometry depicted in Fig 13 resembles an ideal parallel plate configuration. In the ideal case, the uniform field conditions and symmetry allow the plasma problem to be reduced to a one dimensional problem that is easily solved using numerical methods. As mentioned in a previous section, the field at the surface of the probe under ideal conditions can be modelled by the solution to Laplace's equation for a perfectly conducting sphere in a uniform field, i.e.:

$$E_{surface} = E_r = 3E_0 \cos\theta \tag{14}$$

where $E_0$ is the unperturbed uniform field. As evident from the geometry of Fig 13, the actual chamber configuration was not symmetrical; hence field uniformity cannot be assumed.

Given these experimental conditions, the absolute scale factors for each sensor on the probe had to be determined by experimental measurement and numerical modelling of the actual fields at the surface of the probe. Given the computation complexity of obtaining an accurate three-dimensional simulation of the actual electric fields in the chamber, a two-dimensional simulation was instead performed to determine the absolute scale factors of the six probe sensors. In transforming from three to two dimensions, the problem is essentially becomes that of a perfectly conducting cylinder, rather than a sphere. This change in geometry can be approximately accommodated by including a multiplicative constant of 1.5, since surface field on a cylinder in a uniform field is given by $E_r = 2E_0 \cos\theta$. Additionally, the signal from sensors canted relative to the vertical in the actual three dimensional problem must be multiplied by a factor of $\cos(53.5°) \simeq 0.6$ to account for the relative sensor rotation.

The potential distribution in the test chamber was numerically modeled with the plate held at 500V using the finite difference simulation technique. Since the probe was floating in the actual plasma experiments, the plasma free field simulation assumed the probe to float to its local ambient potential.
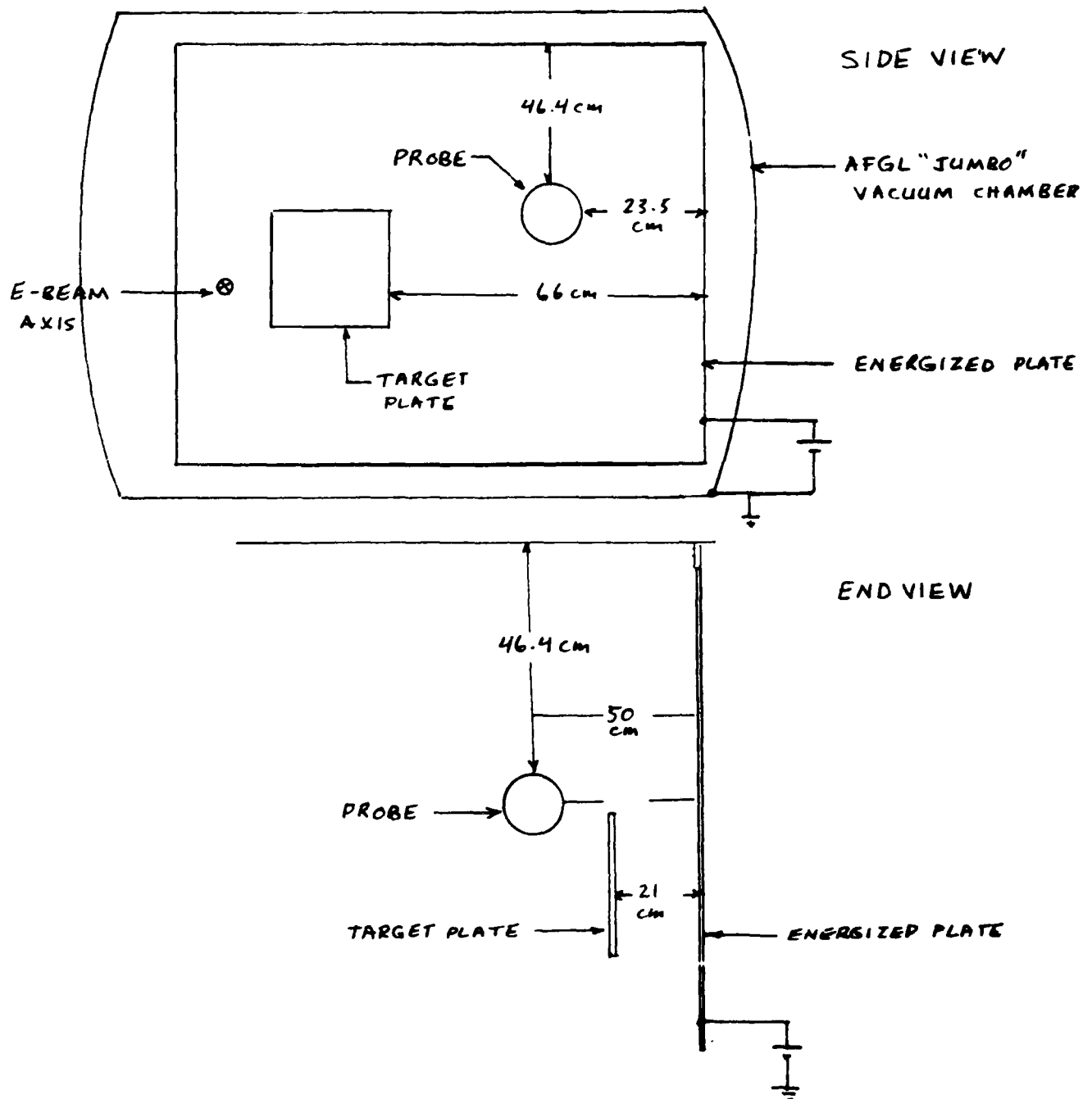
Figure 13 - Layout of the probe and energized plate in the vacuum chamber.

The actual grid layout used in the simulation are shown in Fig 14. As evident from the figure, much of the area in the stimulation is not of use, thus unnecessarily lowering the resolution. To obtain higher resolution, a lower resolution (4 cm) grid was first used to obtain potential values for the points along a square perimeter around the plasma probe. The simulation was then run again at a higher resolution using these potential values for the points along the outer equipotential surfaces, thus providing a higher resolution grid (0.5 cm). From printouts of the fine-mesh simulation, the ambient field in the region of the probe was found to be fairly uniform, and equal to:

$$E_o \simeq 444 \ V/m$$

The resulting values for the two-dimensional surface fields $E_i$ at the projected locations of each sensor are listed in Table 2. The approximate three-dimensional surface fields $E_i'$, computed by multiplying the values of $E_i$ by a factor of 1.5, are tabulated in the second column. The third column lists the relative scale factors $S_i$ of each sensor as determined by direct measurement in a test fixture. These scale factors are expressed in units of a maximum binary count of 256. In obtaining these relative scale factors, a constant field is applied to each sensor individually using a small shielded probe. The measured signals $D_i$ obtained from each sensor in response to a -500V step in plate voltage [2] are shown in the fourth column of Table 2. These signals are also expressed in units of a maximum binary count of 256. Finally, the computed absolute sensitivities $F_i$ of the sensors are shown in the last column of the table. These $F_i$ factors are computed by the relation:

$$F_i = \frac{E_i'}{D_i}$$
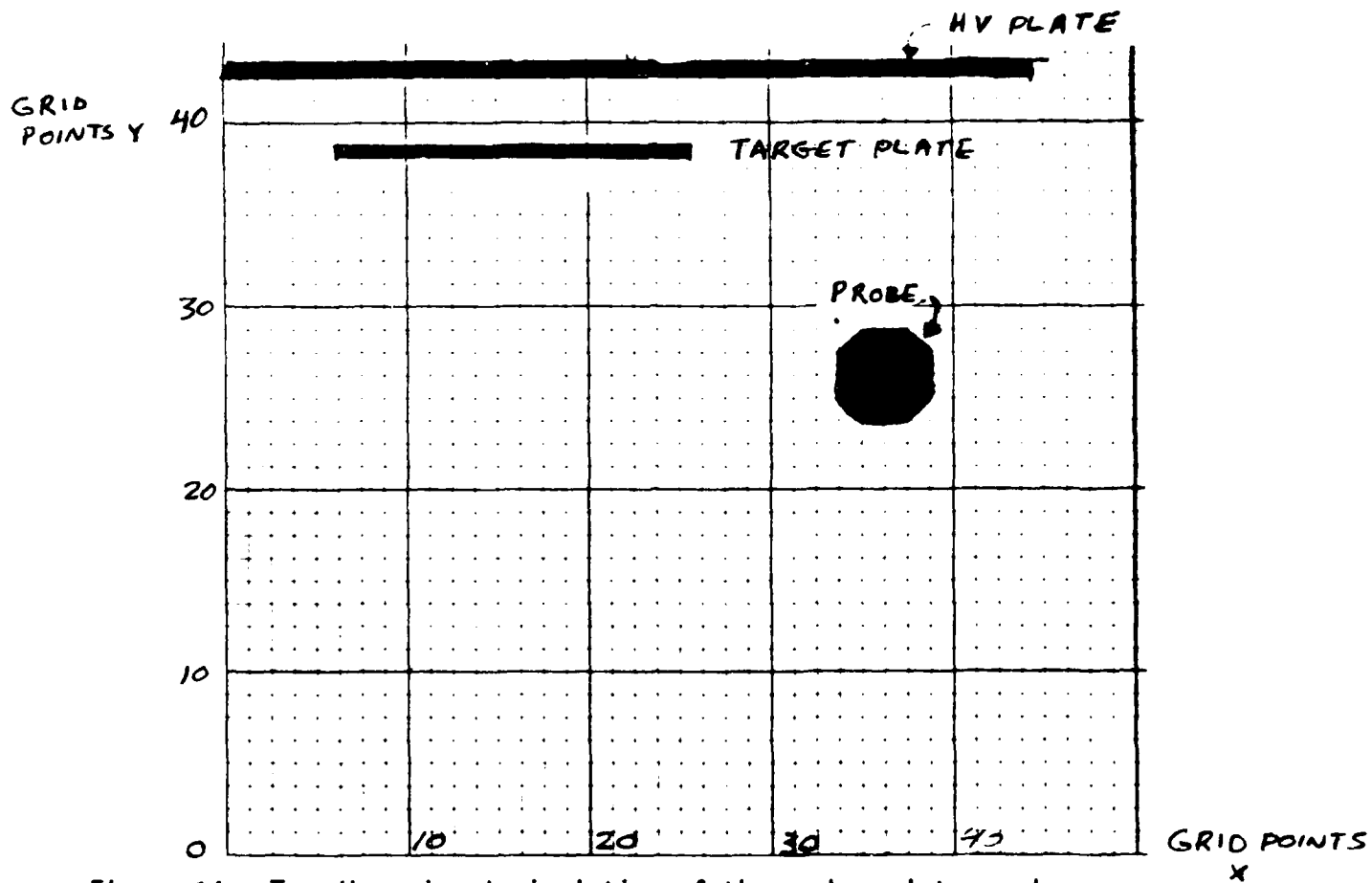
---

2(see pg 98 in the databook)

33

Figure 14 - Two-dimensional simulation of the probe, plate, and vacuum chamber.

Table 2 - Sensor Calibration Measurements From Test Chamber Data

| Sensor # | $E_i$ | $E_i' = 1.5E_i$ | Relative Scale Factor $S_i$ | -500V Step Signal $D_i$ | Absolute Scale Factor $F_i$ |
|---|---|---|---|---|---|
| 1 | 512 V/m* | 456 V/m* | 33 counts | -2.1 counts | 217 V/m per count |
| 2 | 890 | 794 | 125 | 15.4 | 51.6 |
| 3 | 444 | 666 | 72 | -5.6 | 119 |
| 4 | 366 | 549 | 71 | 9.4 | 58.4 |
| 5 | 337 | 506 | 98 | -5.0 | 101 |
| 6 | 370 | 554 | 42 | 3.1 | 179 |

\* The $E_i$ values from sensors #1 and #2 are also multiplied by the factor $\cos 53°$

A check of the measured absolute scale factors $F_i$ against the relative scale factors $S_i$ is provided in Table 3. In the ideal case, each of the products $S_i F_i$ should have the same value. In the third column of the table, the percentage errors relative to sensor #2 (sensor with the largest $S_i$) are indicated.

Table 3 - Product of Relative and Absolute Sensor Scale Factors

| Sensor # | Ratio $S_i/F_i$ | % Difference Relative to Sensor #2 |
|---|---|---|
| 1 | 7160 | 11 |
| 2 | 6450 | 0 |
| 3 | 8570 | 33 |
| 4 | 4146 | -36 |
| 5 | 9900 | 53 |
| 6 | 7520 | 17 |

From the results of Table 3, it is readily apparent that a more accurate means of measuring the absolute sensor scale factors in the vacuum chamber must be found. The results shown in Table 3 do not show good correlation with the calibration experiments run under ideal geometric conditions, as reported in Section 5. The calibration measurements obtained in the vacuum chamber could better be accomplished by either accurate three-dimensional modelling of the fields in the vicinity of the probe or by design of a calibration procedure in which applied sensor fields can be known precisely. One possible design for such a calibration system might involve the construction of a hollow conducting sphere of radius greater than the plasma probe. The calibration sphere would enclose the plasma probe, but be insulated from it. The resulting spherical capacitor could be used to impose known fields at the sensor sites simultaneously.

## 6.5 Plasma Field Simulation Without Plasma Probe

To simplify analysis of the plasma system including the probe, the fields within the plasma can be modelled as a one-dimensional problem. In such a case, Poisson's equation can be solved simultaneously with the electron and ion density functions. Since the ion and electron distributions are a function of potential, Poisson's equation becomes nonlinear, but can be solved using Newton's method [12]. If the electron and ion densities are explicitly included, the one-dimensional Poisson equation becomes:

$$\frac{d^2\phi}{dx} = \frac{-q}{\epsilon_0} [n_i(\phi) - n_e(\phi)] = \frac{-q}{\epsilon_0} n_{tot}(\phi) \qquad (16)$$

Note that the total density $n_{tot}$ is expressed as a function of $\phi$, a necessary step in modelling the properties of the plasma. As noted in the discussion of Langmuir probe theory, the electron and ion densities, in general, will depend on the potential of the plasma relative to the unperturbed ambient. When the plate in the test chamber is negative, so

36

that it is primarily "collecting" ions, the conditions correspond to those used in deriving Eqns (6) and (7), i.e:

$$n_e = n_o \, e^{\phi/V_t}$$

and

$$n_i = n_o \left[ 1 - \frac{2q\phi}{M_i v_o^2} \right]^{1/2}$$

In this case, the sheath edge is a somewhat arbitrary construct since the potential distribution is continuous. In the literature [22,23,24], it is often assumed for computational convenience that the Bohm sheath criterion expresses an equality. Thus Eqn (7) becomes:

$$n_i = n_o \left[ 1 - \frac{2q\phi}{kT_e} \right]$$

For the case of negative plate voltage in the test chamber, Poisson's equation thus becomes:

$$\frac{d^2\phi}{dx^2} = \frac{qn_o}{\epsilon} \left[ e^{\phi/V_t} - \left[ 1 - \frac{2\phi}{V_t} \right]^{1/2} \right] \tag{18}$$

where $V_t = kT_e/q$.

In preparing Eqn (18) for numerical integration, we note that:

$$2 \frac{d\phi}{dx} \frac{d^2\phi}{dx^2} = \frac{d}{dx}\left[ \frac{d\phi}{dx} \right]^2$$

Thus Eqn (18) becomes:

$$\frac{d}{dx}\left[ \frac{d\phi}{dx} \right] = \frac{d\phi}{dx} \frac{2qn_o}{\epsilon} \left[ e^{\phi/V_t} - \left[ 1 - \frac{2\phi}{V_t} \right]^{1/2} \right] \tag{19}$$

37

Integrating Eqn (19) results in:

$$\left[ \frac{d\phi}{dx} \right]^2 = \frac{2qn_o}{\epsilon} \left[ V_t e^{\phi/V_t} + \frac{V_t}{3[1 - 2\phi/V_t]^{1.5}} + C \right] \quad (20)$$

In this equation, C is a constant of integration determined by the boundary conditions at infinity. If it is assumed that the sheath field around the high voltage plate chamber decays to zero before reaching the ground plate (in the one-dimensional case), then the boundary conditions away from the plate can be taken as those at infinity, i.e., as $d\phi/dx = 0$ and $\phi = 0$. It therefore follows that:

$$\frac{d\phi}{dx} = \frac{2qn_oV_t}{\epsilon} \left[ e^{\phi/V_t} + \frac{1}{3(1 - 2\phi/V_t)^{1/2}} - \frac{4}{3} \right]^{1/2} \quad (21)$$

It is important to note that Eqn (21) was derived by assuming that ion sheath formed around the negatively energized plate. For the case of a positive plate, an electron sheath forms, and a second derivation must be performed to find the ion and electron densities as a function of potential. Such a derivation can be based, in part, on the Child-Langmuir formulation for space-charge limited electron current. In performing this derivation, the plasma chamber is again modelled as two infinite parallel plates.

It is first assumed that the plate potential is large enough so that almost all the ions are repelled; their distribution, if originally Maxwellian with the probe present, is given by:

$$n_i(\phi) = n_o e^{\phi/V_t} \quad (22)$$

The electrons will be accelerated by electric field with velocity:

38

$$v_e = \left[ \frac{2q\ \phi(x)}{m_e} \right]^{1/2} \tag{23}$$

Equation (23) assumes that collisional effects can be neglected. Under these conditions, the current density becomes:

$$J = qn(\phi)\ v_e(\phi)$$

so that the electron density becomes:

$$n_e(\phi) = \frac{J}{q} \left[ \frac{2q\phi}{m_e} \right]^{1/2} \tag{24}$$

For the case of electron space-charge limited current in one-dimensional geometry, Langmuir found the following relationship: [12]

$$J = \frac{4q\epsilon}{9}\ \frac{2}{m_e q} \left[ \frac{(V - V_m)}{(d - x_m)} \right] \left[ 1 + \frac{2.66}{(V/V_t)^{1/2}} \right] \tag{25}$$

where d is plate spacing, and V is the applied plate voltage. The constants $V_m$ and $x_m$ are empirical correction factors. It has been found [23] that for practical cases $V_m$ and $x_m$ are small and may be neglected, as is done in this derivation. Substituting Eqn (25) into Eqn (24) results in:

$$n_e(\phi) = \frac{4}{9}\ \frac{\epsilon\phi}{(qd)^2} \left[ 1 + \frac{2.66}{(V_t/\phi)^{1/2}} \right] \tag{26}$$

The same steps are performed as in the previous derivation for the ion sheath, resulting in:

$$\left[ \frac{d\phi}{dx} \right]^2 = \frac{2q}{\epsilon} \left[ \frac{4}{9}\ \frac{\epsilon}{(qd)^2}\ [\phi^2/2 + 1.77\phi^{1.5}\ V_t^{1/2}] + C \right] \tag{27}$$

where C is a constant. Since $\phi = 0$ at $x = \infty$, it follows that:

$$\frac{d\phi}{dx} = \left[ \frac{4}{9d^2} \left[ \phi^2 + 31.92 V_t^{1/2} \phi^{1.5} \right] - \frac{2qnV_t}{\epsilon} e^{-\phi/V_t} + 1566.3 \right]^{1/2} \tag{28}$$

This equation was solved numerically for several values of a plate voltage between -500V and +500V, using the plasma parameters found in Section 6.3. The source code of the sheath simulation program is found in Appendix A. The results show that the fields originating on the energized plate do not decay to zero before reaching the ground plate. Note that solving for the sheath fields, including the boundary conditions at the ground plate, where a sheath region will also form, requires more sophisticated numerical methods than those used here. The sheath region surrounding the ground plate will extend only on the order of a Debye length into the space between the plates. As previously calculated, the Debye length is equal to $\lambda = 15$ cm if the electron temperature is equal to $T_e = 9.5eV$ and the plasma density to $n_0 = 4.56 \times 10^9/m^3$. Thus, in the region occupied by the spherical probe, i.e. on the order of a meter from the ground plate, the perturbation due to the ground plate will be minimal.

The fact that the plasma probe, located about 50 cm from the energized plate, is well within the sheath region could explain an unexpected effect observed during Langmuir probe tests. When the Langmuir probe data was taken (see Fig 11), the slope of the I-V curve for $V > 0$ was inversely proportional to the voltage applied to the plate. For regions well within the sheath of the energized plate, $n_e$ will be greater than $n_i$, and $n_e$ will decrease for positions farther into the sheath region. The current to the Langmuir probe is proportional to $n_e$ in region A of Fig 10, however. Therefore, the probe current in region A will be inversely proportional to the plate voltage.

## 6.6 Saturation Effect With Probe Present in Plasma

When plasma was introduced into the chamber with the probe present, some sensors exhibited an exponential-like response curve, as depicted in Fig 15 for sensors #4 and #6.



sensor 6
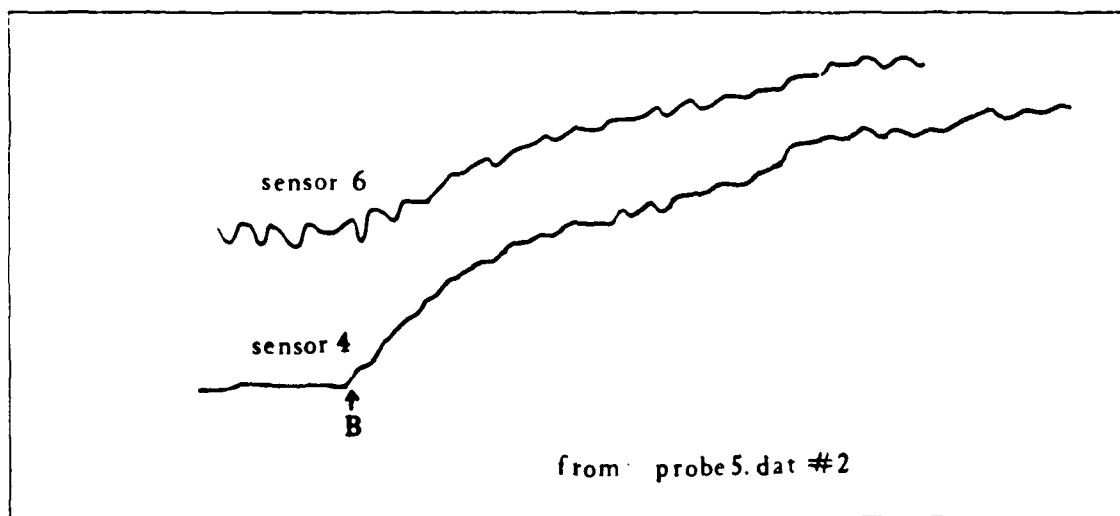
sensor 4

B

from probe5.dat #2

Figure 15 - Output from sensors #4 and #6 as a function of time

The following theory is proposed to explain this undesired anomaly: The surface field sensors are imbedded in a potting compound which encloses the sensor electronics and related components. Only the outer surface of the sensing electrode is exposed via the sensor aperture on the surface of the sphere. The exposed surface of the insulating dielectric is capable of collecting surface charge. It was hypothesized that surface charge of large enough magnitude (either ion or electron) was being deposited on the dielectric to cause the observed sensor saturation effect.

The curves of Fig 15 were plotted on a semi-log scale using least squares methods in order to verify the hypothesis that the curves were exponential. The resulting plots are shown in Fig 16. From the least squares analysis of x versus $\ln(y_{max} - y)$, the time constants and correlation coefficients for sensors #2 and #6 were obtained, and are listed in Table 4.
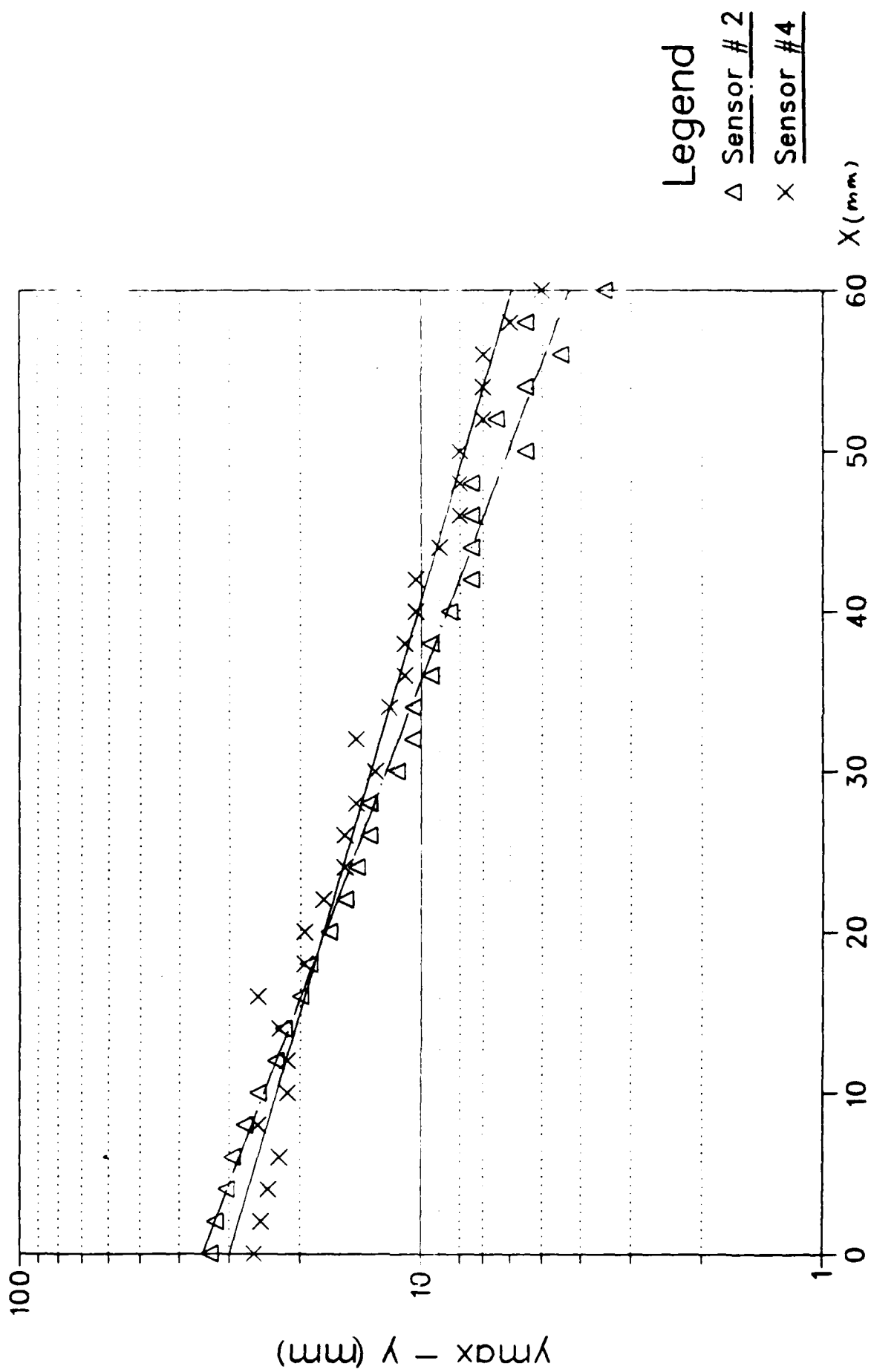
Figure 16 - Charging curves of sensors #2 and #4 measured after initiation of the plasma in the vacuum chamber. The vertical scale is logarithmic.

Table 4 - Measured Sensor Saturation Time Constants (Sensors #2 and #6)

| Sensor # | seconds | correlation coefficient |
|----------|---------|-------------------------|
| 2 | 46.2 | -0.993 |
| 6 | 72.6 | -0.984 |

From the correlation coefficients in Table 4, it was concluded that the probe-plasma interaction did exhibit an exponential dynamic response. A simple theoretical model, based on the sensor geometry of Fig 17, was developed to explain the initial saturation charging curves of Fig 15. The model also yielded a quantitative value for the exponential time constant which compares favorable with the measured values listed in Table 4. In formulating the model, the following assumptions were made:

1) The initial surface charge on the dielectric is zero.

2) The area of the surface field electrode is negligible in comparison to the area of the dielectric (i.e., ($r_d \gg r_s$) so that most of the charge collects on the dielectric.

3) The current density J, when present, is uniform into the surface of the dielectric.

4) The dielectric constant of the potting compound is much greater than $\epsilon_0$.

5) The dielectric constant of the plasma is equal to $\epsilon_0$ (zero magnetic field case).

6) The ion current is negligible (zero ion temperature approximation).

The introduction of plasma into the chamber is modelled as a step in charge at the probe surface (x = 0). Due to assumption (6) and the fact that the probe is at the plasma potential, only the electron diffusion term becomes non-zero in the current equation. The electron surface charge which collects on the dielectric causes an electric field, which, in turn, causes a deceleration of the electrons. The latter can be modelled as a drift term in the current equation. The accumulated surface charge is related to the current density normal to the dielectric surface, as expressed by:
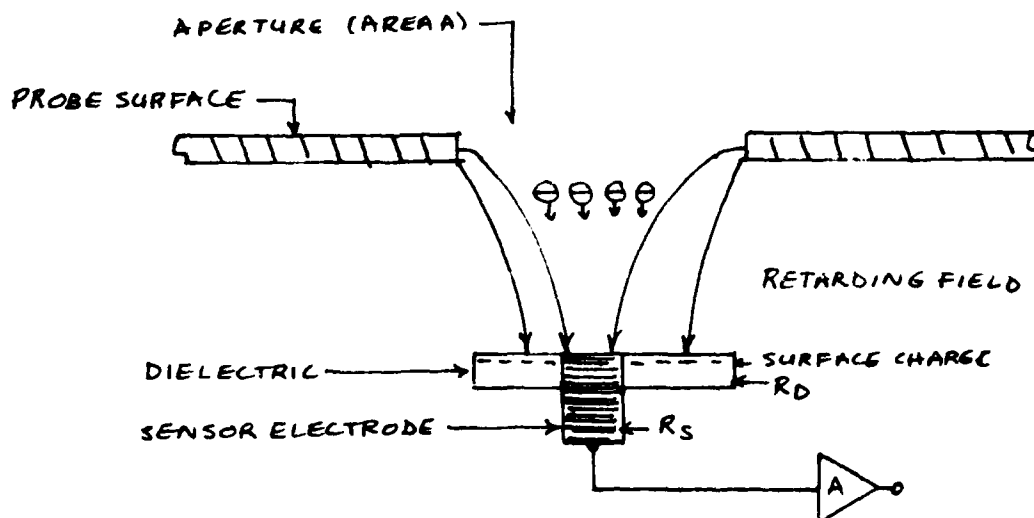
$$d\sigma = J \, dt$$

43

Figure 17 - Physical model for sensor charging

If $\epsilon_{pot} \gg \epsilon_o$, then the field associated with this surface charge will be given by:

$$E \simeq \frac{\sigma}{\epsilon_{pl}} = \frac{\sigma}{\epsilon_o} = \int \frac{d\sigma}{\epsilon_o} = \int \frac{Jdt}{\epsilon_o}$$

The time rate of change in the electric field is thus given by:

$$\frac{dE}{dt} = \frac{J}{\epsilon_o} = \frac{-q}{\epsilon_o} \left[ n\mu_e E - D_e \frac{dn}{dx} \right] \tag{29}$$

or

$$\frac{dE}{dt} + \frac{qn\mu}{\epsilon_o} E = \frac{-qD_e}{\epsilon_o} \frac{dn}{dx} \tag{30}$$

where $\mu_e$ is the mobility of the electrons and $D_e$ the diffusion constant of the electrons. From reference [25], the mobility of electrons in Argon gas at $2.5 \times 10^{-4}$ Torr (the Argon neutral pressure in the chamber) was taken to be $\mu_e = 3.33$ cm$^2$/V-s. Similarly, the diffusion constant was

44

taken to be $D_e = KT_e/q = 21.66$ cm$^2$/s. A time constant results from the homogeneous solution to Eqn (30), given by:

$$\tau = \frac{\epsilon_0}{qn\mu_e} = 36.4 \text{ s}$$

This theoretical time constant is in good agreement with the measured values given in Table 4. It is likely that even better agreement between theoretical and actual values could be achieved for the condition $r_d \simeq r_s$. In this latter case, not all current entering the sensor aperture would reach the dielectric and the theoretical time constant would increase. Based on the assumption that the dielectric charging model is a reasonable approximation of the saturation effect, corollaries to the dielectric charging model were developed in order to predict saturation charging of the sensors when potentials were applied to the high-voltage plate.
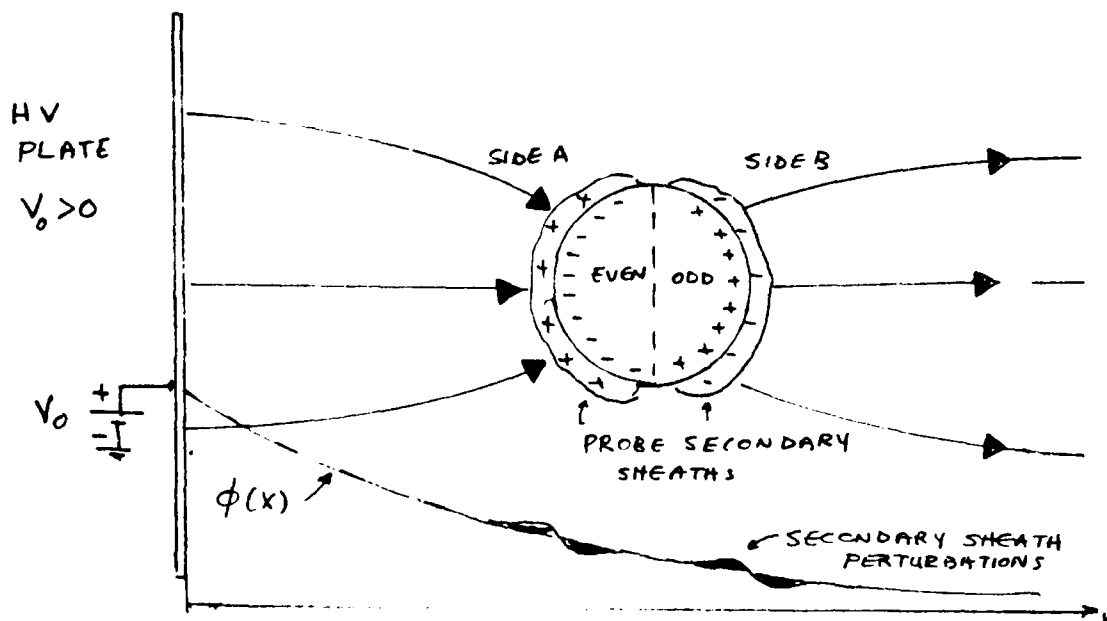


Figure 18 - Model for plasma charging of the sphere in the test chamber

This situation is depicted in Fig 18. When a positive potential is applied to the high-voltage plate, field lines terminate on the side of

the probe containing the even-numbered sensors (side A) and field lines originate on the side containing the odd-numbered sensors (side B). Thus side A will have a net negative surface charge and side B will have a net positive surface charge. When field lines originate on a sensor electrode, the sensor output signal increases. Conversely, when field lines are terminated on a sensor electrode, the sensor output signal decreases. Given the orientation of the probe sphere in the experimental setup of the vacuum chamber, it follows that the net output signal from even numbered sensors should be negative, and the net output signal from odd numbered signals should be positive when a positive voltage is applied to the energized plate.

Due to the net surface charge on the probe, the sheath regions for the even and odd numbered sensors will be of a fundamentally different nature: an ion sheath will exist on side A and an electron sheath will exist on side B. When the sheath charge enters the sensor apertures and collects on the potting dielectric it will cause an added surface charge on the electrode of the opposite sign. Thus the effects due to the termination of the field lines and the accumulation of saturation charge will be additive.

When a potential is applied to the high-voltage plate there will thus be an immediate discontinuity in sensor signal due to the termination of the field lines on the probe, followed by a saturation process where some asymptotic value is reached with a time constant on the order of 30s. When the plate voltage is switched from 500V to 0V, the even-numbered sensors are observed to saturate upward while the odd-numbered sensors saturate downward. This result could be explained using the above model by noting that when the plate voltage equals 0V, the dielectrics of the even-numbered sensors have become positively charged with respect to the plasma and thus attract electrons from the plasma. This net electron flux to the dielectrics will in turn cause an upward drift in the readings. The downward drift in sensor #1 can be explained with the same reasoning if the negatively charged dielectric is considered to attract positive ions. The initial discontinuity is of primary interest since from it can be determined the surface field on the probe due to the potential applied to the high- voltage plate. The magnitudes of these discontinuities, as well

as the corresponding jumps in surface field values, are listed in Table 5 for plate voltage steps of 100V over the range 0 - 500V. Because of the observed saturation effects, only a limited number of data values were obtainable for each sensor.

Table 5 - Change in Sensor Readings versus Change in Applied Plate Voltage

| Sensor # | Plate Voltage Change | Sensor Output | Surface E-field Change |
|----------|----------------------|---------------|------------------------|
| 1 | 0 - 100 V | 8.0   cnts | 1562 V/m |
| 1 | 100 - 200 | 6.67 | 1302 |
| 2 | 100 - 200 | -4.44 | -229 |
| 2 | 200 - 300 | -5.33 | -275 |
| 4 | 300 - 400 | -4.44 | -403 |
| 4 | 400 - 500 | -4.88 | -443 |
| 4 | 500 -   0 | 14.65 | 1329 |
| 6 | 0 - (-100) | 2.79 | 427 |

## 6.7 Secondary Sheath Surrounding Probe

As shown in Fig 18, when the probe is inserted into the plasma sheath, secondary sheath regions will form around the probe. In order to obtain accurate quantitative values for the effect these secondary sheaths cause on the readings, the two-dimensional, nonlinear Poisson and charge conservation equations must be solved simultaneously. As a means of simplifying the problem, it will be assumed that nonlinearities are negligible (an unverified assumption), so that the system can be modelled using superposition. If superposition of the primary and secondary fields is applicable, then the one-dimensional simulation, with the plate voltage set to 500V, for example, yields a field of $E_0$ = 399 V/m at the position of the probe. Converting this result to three dimensions yields a probe surface field of:

$$E_s = 3E_0 \cos(53.5^\circ) = 711 \text{ V/m}$$

The spherical probe will take on the potential of the undisturbed plasma measured at the location of the sphere's center. There will thus be a potential difference $V_{pp}$ between the surface of the probe (7.5 cm from its center) and the potential that would exist in the undisturbed plasma, resulting in a secondary sheath surrounding the probe. Using the values obtained from the one-dimensional sheath simulation with the plate voltage set to 500V, the difference in potential between the location at the probe's center and location at its surface is found to be about 29V. Converting to the equivalent three dimensional case yields the value $V_{pp}$ = 87V. Using Eqn (26), $n_0$ was calculated at the probe surface for $E_0$ = 398V/m, resulting in the value $n_0$ = 1.88 x $10^{10}$/m$^3$.

The surface field $E_s$' due to the secondary sheath surrounding the probe was calculated using Eqn (21) with $n_0$ = 1.88 x $10^{10}$/m$^3$ and the initial potential $\phi = V_{pp}$ = 87V, yielding the result:

$$E_s' = 417 \text{ V/m}$$

Assuming superposition holds, the total field at the surface of the probe becomes:

$$E_{tot} = E_s + E_s' = 711 + 417 = 1128 \text{ V/m}$$

As indicated in Table 4, the measured field value obtained from Sensor #4 was 1329 V/m, i.e. the predicted and measured field values differ by about 15%.

For the case of the measurements taken from sensor #1 or #6 in Table 4, an electron sheath is formed around the sensors as opposed to an ion sheath for sensors #2 and #4. The theoretical model for the surface field due to the secondary electron sheaths was developed using the distribution function for electron collection with a spherical probe in the thick sheath limit [23]. For $\phi \gg V_t$, the electron density is given by:

$$n_e \simeq qn_o \frac{\phi}{V_t}$$

so that the approximate Poisson's equation becomes:

$$\frac{d^2\phi}{dx^2} \simeq \frac{qn}{\epsilon} \frac{\phi}{V_t}$$

Applying the same development used on Eqns (21) and (27) results in:

$$\frac{d\phi}{dx} = \frac{qn}{\epsilon V_t}$$

The surface field for sensor #6, with $\phi = V_{pp} = 18.9$ V, can thus be calculated:

$$E_s = 3 \ (81.9) \ \cos \ (53.5^\circ) = 146 \ V/m$$

and

$$E_s' = (18.9 \ V) \ (3/m) = 56.7 \ V/m$$

or

$$E_{tot} = E_s + E_s' = 203 \ V/m$$

As indicated in Table 4, the measured value of $E_{tot}$ for sensor #6 was 427 V/m, i.e. the predicted and measured field values differ by about 52%.

For sensor #1, with $V_{pp} = 19.8V$:

$$E_s = 3(87.5) \ \cos \ (53.5_o) = 156 \ V/m$$

and

$$E_s' = 59.4 \ V/m$$

or

$$E_{tot} = 215.6 \ V/m.$$

For sensor #1, the measured and theoretical values differ by approximately a factor of six.

The large discrepancy between theoretical and measured values for sensors #1 and #6 could be explained by the fact that for both sensors the secondary sheaths were electron sheaths. The detection electronics averages the signal over a period of approximately one-second. During this one-second interval, however, charge is being deposited on the dielectric surfaces surrounding the sensors. Since the mobility of the electrons is much greater than that of the ions, the effects due to the secondary electron sheath should also be seen sooner than the effects due to the secondary ion sheath. It is hypothesized that for sensors surrounded by secondary electron sheaths non-negligible dielectric charging effects occur during the first detection period before E-field values can be output.

# 7. CONCLUSION

The experiments reported here show that it is indeed possible to build a free floating, self-contained spherical electric field probe capable of measuring both volume field magnitudes and the amount of collected probe charge. These quantities can be useful in evaluating the parameters of the plasma sheath surrounding the spherical probe.

Models for simulating both static and dynamic plasma conditions within the test chamber have been developed. The time constant for the saturation effect which dominates probe behavior was predicted by theoretical models to be within 30% of the actual measured value. Electric field readings for secondary ion sheaths were predicted with an accuracy of 15%. This relative small value for the error in E-field prediction indicates that with suitable knowledge of plasma conditions more accurate calibration factors can be determined for the sensor readings.

Further directions for work on the probe include:

1. Development of simpler, more accurate methods for calibrating the probe, and determining the absolute scale factors. One possibility might be to use a concentric spherical electrode for establishing a known field.

2. Redesign of the sensor modules to eliminate the observed saturation effect caused by the buildup over time of charge on the dielectric surrounding the sensor electrode during plasma tests.

3. Modification of the plasma density and electron temperature to test the robustness of the sheath simulation, and to more closely approximate the plasma in low earth orbit.

## 8. ACKNOWLEDGEMENTS:

## 9. REFERENCES

1. M. Misakian, F.R. Kotter, and R. Kahler, "Miniature ELF Electric Field Probe", Rev Sci Instrum, 49 ,(1978), pp 933-935.

2. H. Bocker and L. Wilhelmy, "Messung der Elektrischen Feldstarke bei hohen Transienten und Periodisch Zeitabhangigen Spannungen", ETZ-A, Bd. 91, (1970) H.8, pp 427-430.

3. R. Spiegel, D. Derns, E. Cooper, Jr, and E. Bronaugh, "Small Accurate Optically Isolated Electric Field Probe", I.E.E.E. Power Engineering Society, Summer Meeting, paper A 79-507-5, Vancouver, B.C., July 1979.

4. H. Bocker and E. Hagenmeyer, "Ein Beitrag zer Messung der Elektrischen Feldstarke bei hoher Gleichspannung", ETZ-A, Bd. 87 (1966), H.23, pp 829-831.

5. L. Collins, Y. Linde, and S. Self, "Spherical Probes for Corona Discharges", Journ. of Electrostatics, 4 , (1978), pp 377-389.

6. P. Moon and D. Spencer, Field Theory for Engineers, Princeton, NJ: D. Van Nostrand Co, Inc, 1961. pp 372-376.

7. J.R. Melcher, Continuum Electromechanics, Cambridge, MA: MIT Press, 1981.

8. M. Zahn, Electromagnetic Field Theory, New York: John Wiley and Sons, 1979, pp 293-297.

9. F. Whipple and J. Chalmers, "On Wilson's Theory of the Collection of Charge by Falling Drops", Quart. Journ. of the Roy. Met. Soc., 70, (1944),pp 103-119.

10. M. Pauthenier and M. Moreau-Hanot, "La Charge des Spheriques dans un Champ Ionise", J. Phys. Rad., 3, (1932), p 590.

11. H. White, Industrial Electrostatic Precipitators, Reading, MA: Addison-Wesley, 1963.

12. Rosen, A. ed, Spacecraft Charging by Magnetospheric Plasmas, Progr. in Astro and Aero Series, vol 47, MIT press 1975

13. Garrett, H.B., "The Charging of Spacecraft Surfaces", Rev. Geophys, vol 19, no 4, 1981, p 577.

14. Parker, L.W., "Wakes and Differential Charging of Large Bodies in Low Earth Orbit", Spacecraft Environmental Int Tech, AFGL-TR-85-0018, 1983, p 235.

15. Fahleson, U. Space Science Review, 7, 1967, pp 238-262.

16. Boyd, R.L.F, ibid, pp 230-237.

17. Persson, H. ibid, pp 228-229.

18. Wildman, P.J.L., Jour of Atmos and Terr Phys, 27, 1965, pp 417-423.

19. Currie, D.R. and Kreilsheimer, K.S., Jour of Atmos and Terr Phys, 1960, pp 126-135.

20. Horenstein, M.N., private communication.

21. Shohet, J.L., The Plasma State, Academic Press, New York, 1971.

22. Chen, F.F., Intro to Plasma Physics and Controlled Fusion, Plenum Press, New York, 1984.

23. Chen, F.F., "Electric Probes:, Chap 4 in Huddlestone, R.H. and Leonard, S., Plasma Diagnostic Techniques, Academic Press, New York, 1965.

24. Swift, J.D. and Schwarz, M.J.R., Electrical Probes for Plasma Diagnostics, American Elsevier Pub Co., New York, 1969.

25. Brown, S.C, Basic Data of Plasma Physics, Wiley, New York, 1959.

26. Pierce, J.M., "Electric Field Measurement in a Plasma Sheath", Directed Study Final Report, Boston University ECS Dept., Nov 1985, BUTR-85-3752.

27. Corliss, W.R., Scientific Satellites, NASA SP-133, 1967, pp 461-463.

28. Brace, L.H., and Spencer, N.W., "First Electrostatic Probe Results from Explorer 17", Journ Geophys Res, 69, 1964, pp 4686-4689.

29. Flatley, T.W., and Evans, H.E., "The Development of the E-field Meter for the Explorer VIII Satellite", NASA TN D-1044, 1962, p 81.

30. Krall, N.A. and Trivelpiece, A.W., Principles of Plasma Physics, McGraw Hill, New York, 1973.

31. Nicholson, D.R., Introduction to Plasma Theory, Wiley, New York, 1983.

32. Tanenbaum, B.S., Plasma Physics, McGraw Hill, New York, 1967.

33. Mitchner, M., and Kruger, C.H., Partially Ionized Gases, Wiley, New York, 1973.

34. Alder, B., and Fernbach, S., eds, Methods in Computational Physics, vol 9 : Plasma Physics, Academic Press, New York, 1970.

## APPENDIX A - SOURCE CODE OF PROBE MICROPROCESSOR

```
C*********************************************************************
c                              SHEATH
c CALCULATES E-FIELD AND POTENTIAL BETWEEN PARALLEL PLATES IN A PLASMA
c
C*********************************************************************
c set constants in mks
      eps= 8.85e-12
      pi= 3.14159
      q= 1.6e-19
c
c set plasma parameters
      vtherm= 40.
      dens  = 1.e12
c
c set plate voltage
      vplate = -500.
c
cset integration constants
      write(5,98)
98    format(' input value of dx in meters, #max ("print every #")')
      read(5,97) dx,max
97    format(f20.15,i10)
c
c initialize integration:
      m=0
      x=0.
      phi=vplate
      cosh= (exp(phi/vtherm) + exp(-phi/vtherm))/2.
      e= -sqrt(4.*vtherm*q*dens*(cosh-1)/eps)
      write(5,103)e,phi
103 format(' initial field:',f15.1,5x,'initial pot:',f10.2)
c
c
c begin integration
300 continue
      m=m+1
      sinh= (exp(phi/vtherm) - exp(-phi/vtherm))/2.
c
      phi = phi - e*dx
      e = e + (-dens*q*2.*sinh/eps)*dx
      x=x+dx
c
      if(m.lt.max) go to 300
      write(5,200) m,x,phi,e
200 format(' ',i10,'    x=',f10.8,'  pot= ',f15.1,'    E= ',f15.1)
      m=0
      goto300
      end
```

APPENDIX B - DETAILS OF PROBE MODULES AND COMPONENTS
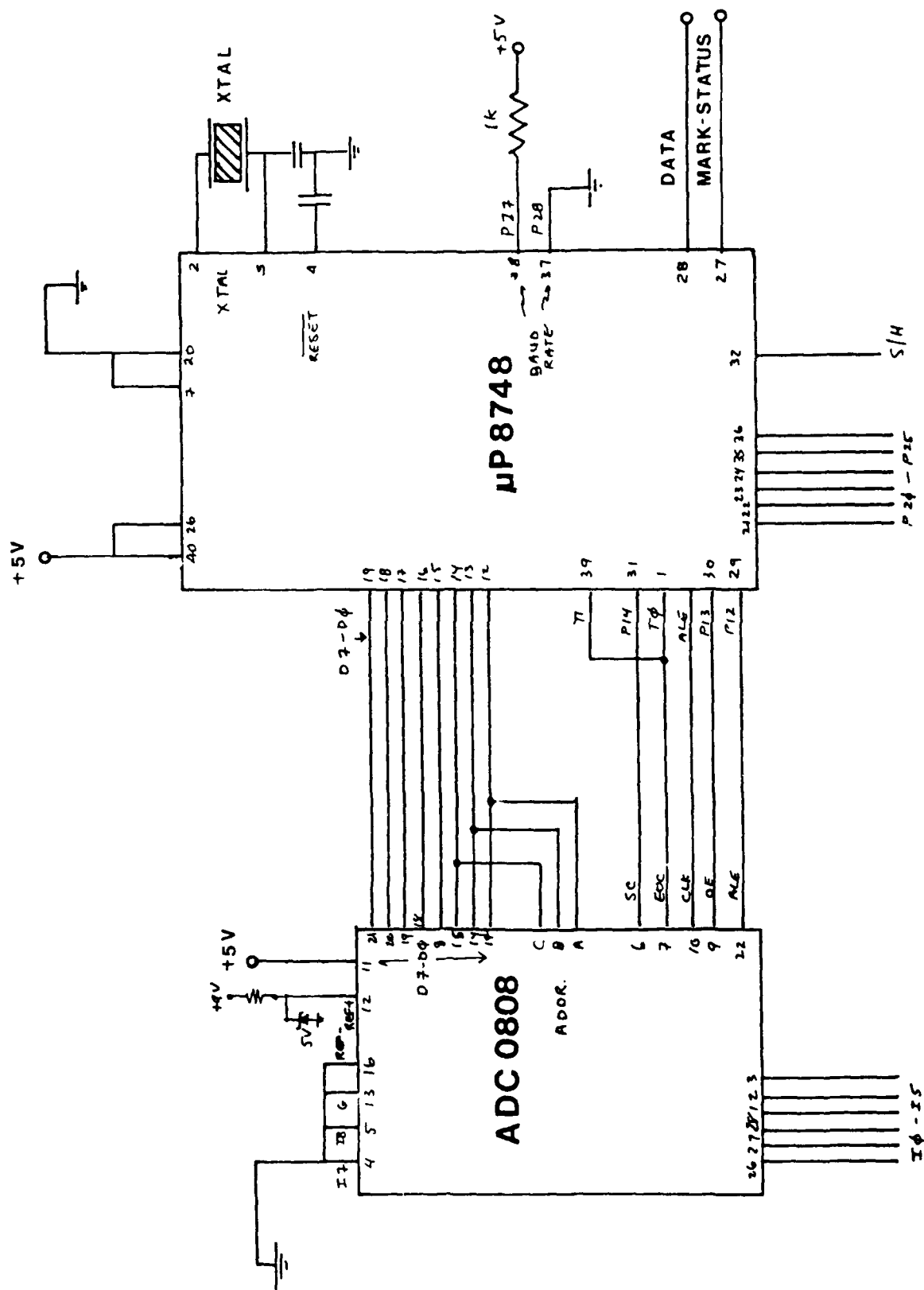
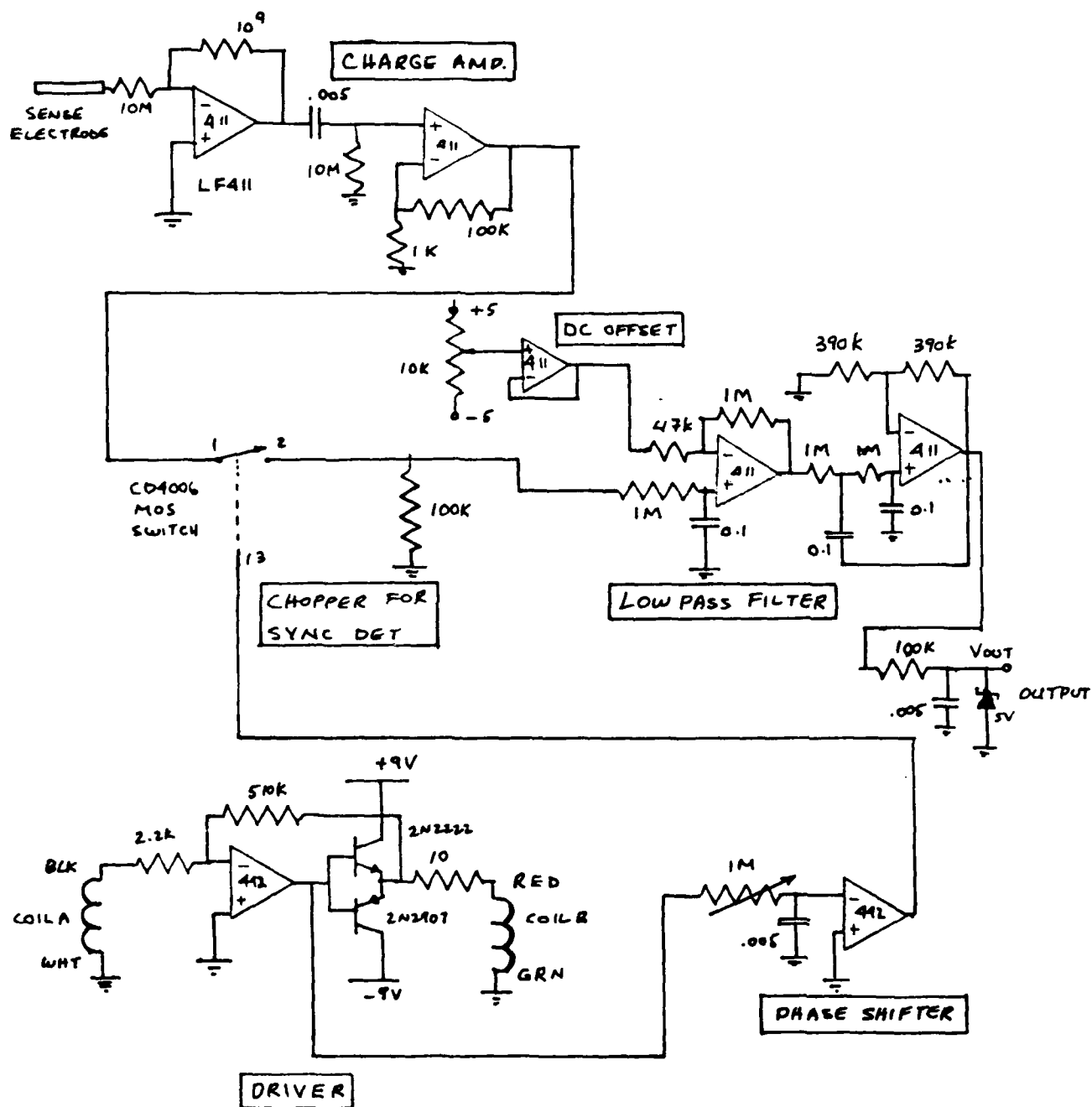Figure A1 - Microprocessor and Analog to Digital Converter Boards Located Inside Sphere.

58

Figure A2 - Analog Processing Circuitry which samples field mill sensors and converts to dc signals sent to A/D converter. Six such systems make up the complete probe; one for each of the six sensors.
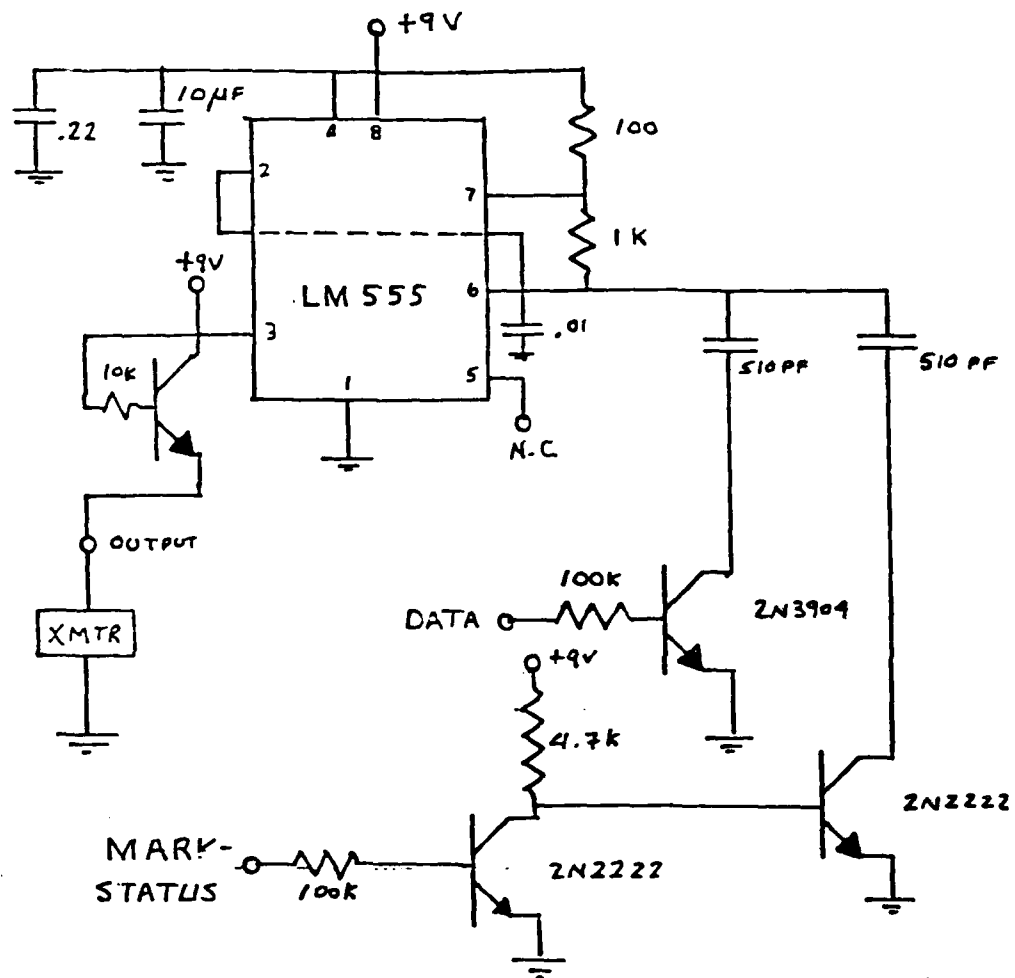
Figure A3 – Frequency Shift Keyed, Amplitude Modulated (FSK-AM) interface
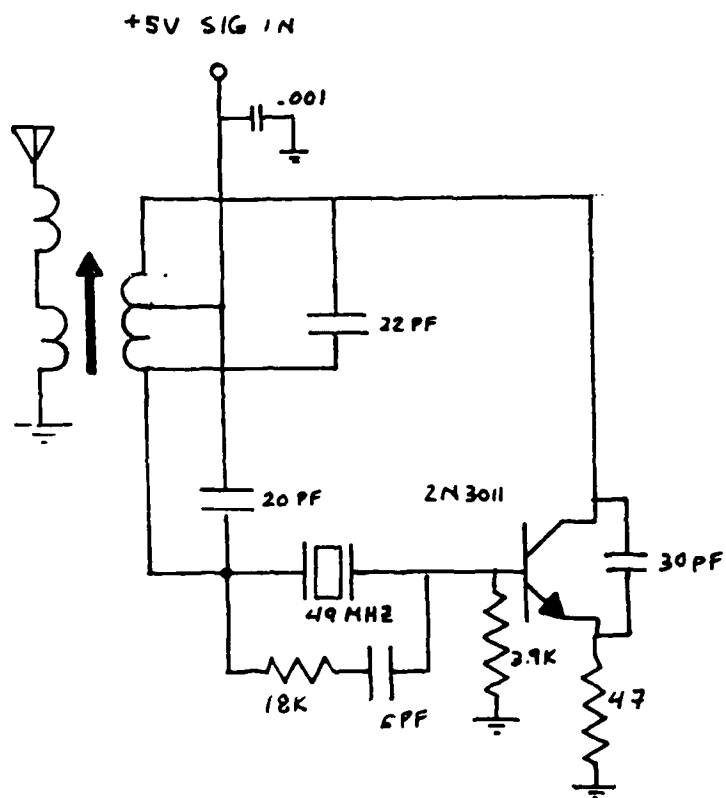between microprocessor and rf transmitter.

60

Figure A4 - 49 MHz rf transmitter and antenna coupling transformer.
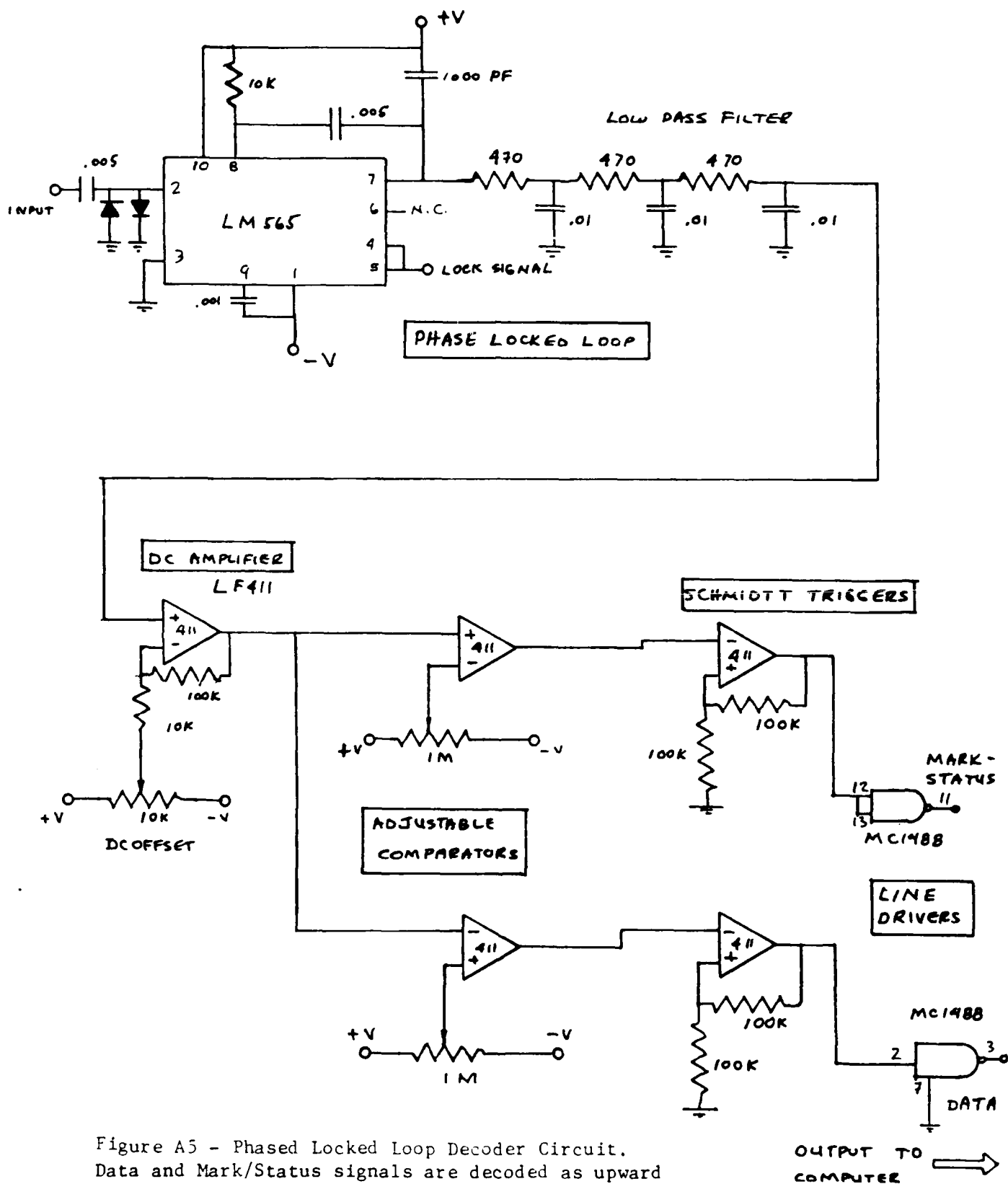
Figure A5 - Phased Locked Loop Decoder Circuit. Data and Mark/Status signals are decoded as upward and downward shifts respectively in received FSK frequency.

FIGURE A6

SPHERE SIDE VIEW

63
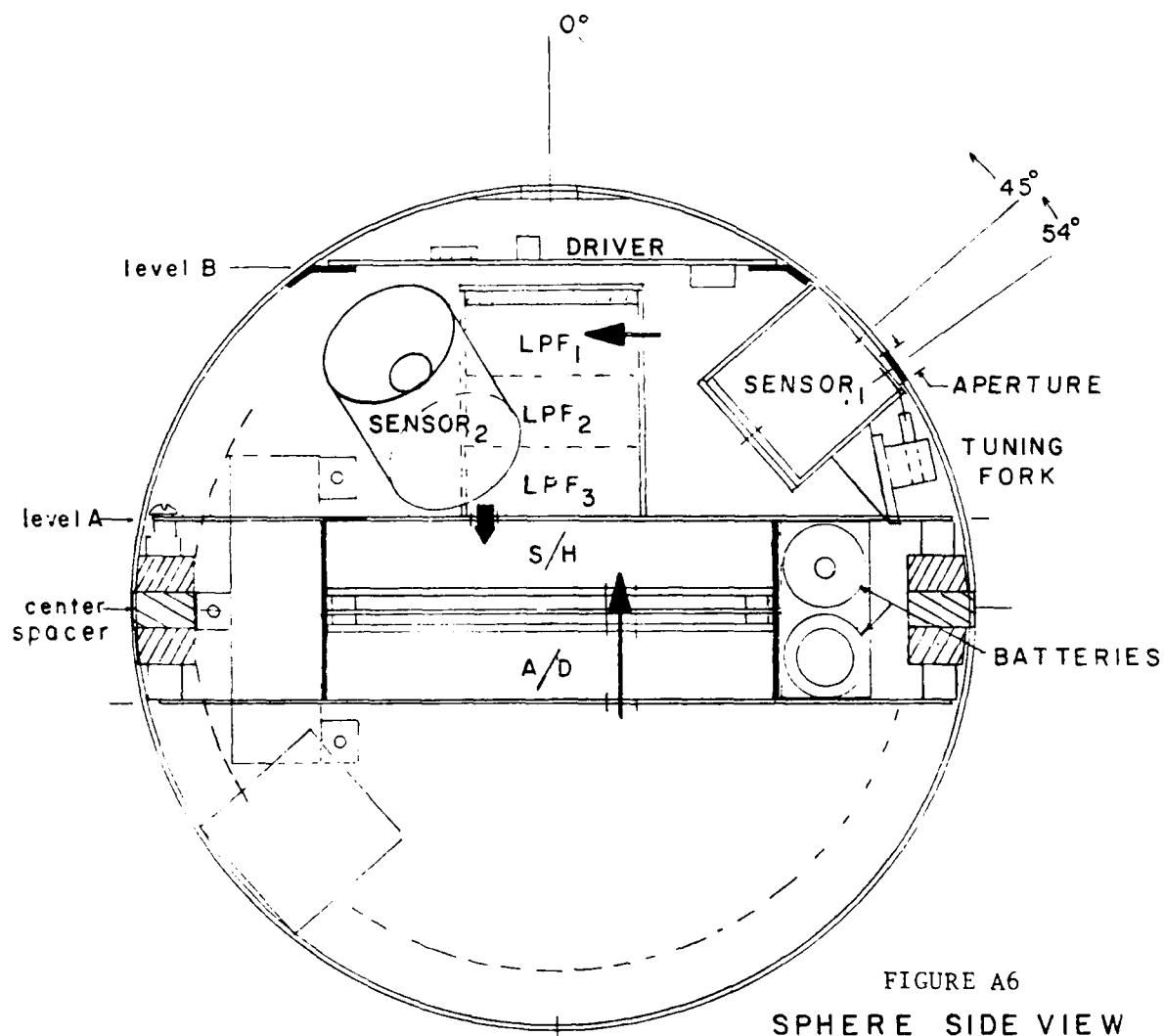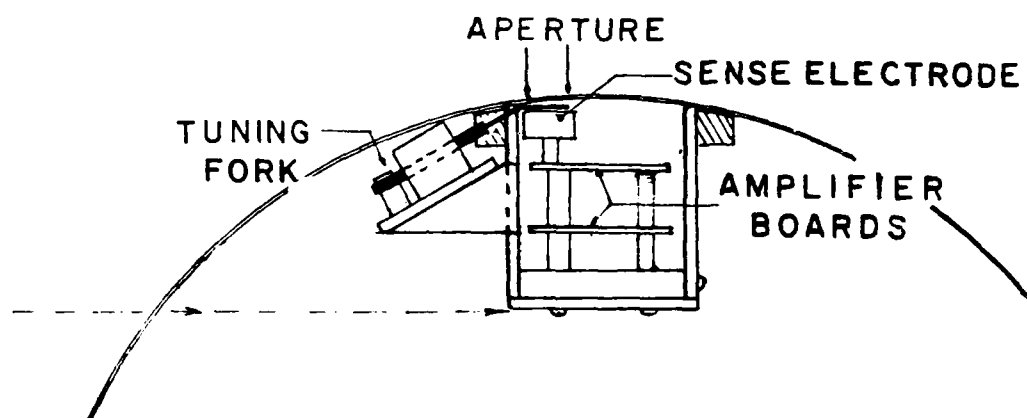
Figure A7 - Details of Field Mill Chopper located at each sensor
aperture.
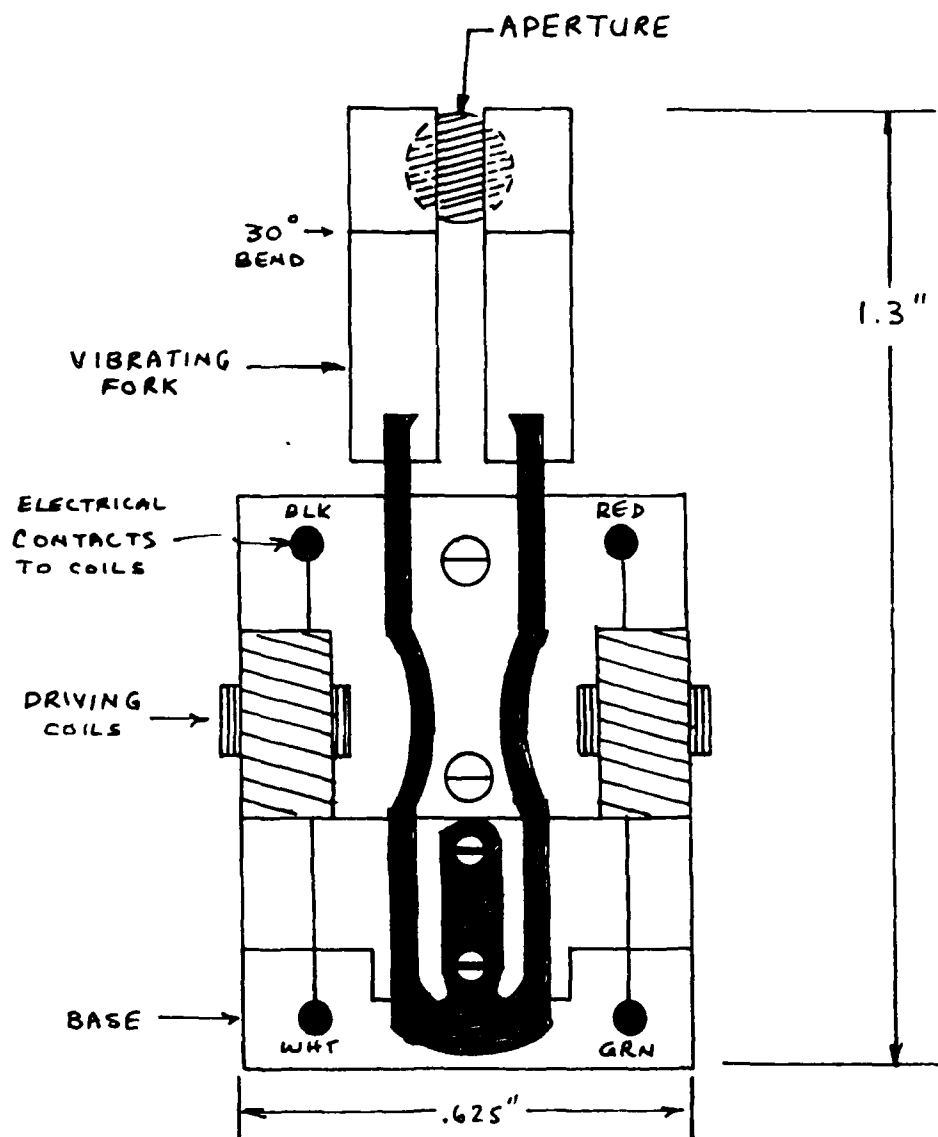
Figure A8 - Magnified detail of tuning fork chopper used to drive field
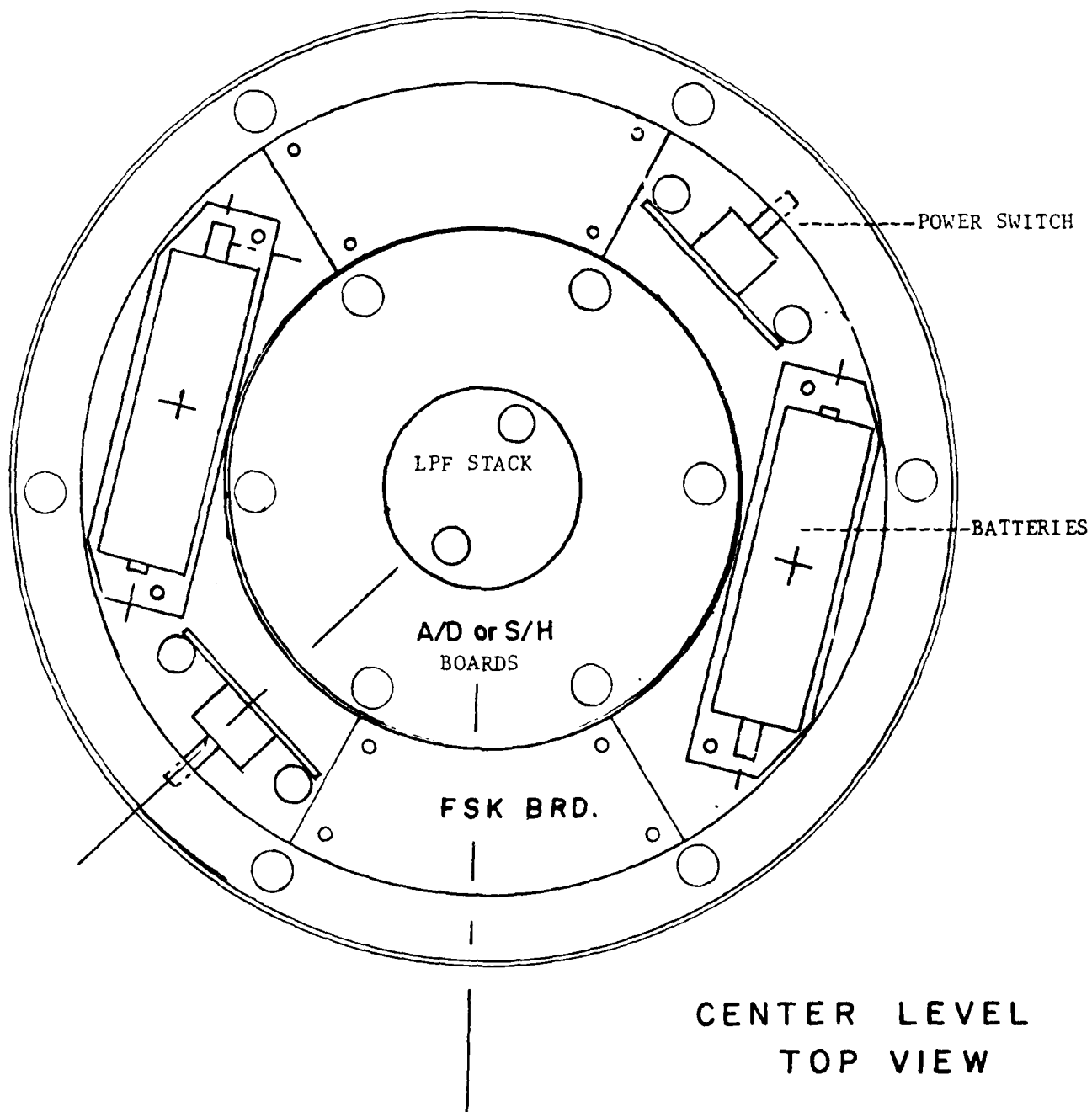mill sensors. (American Time Products).

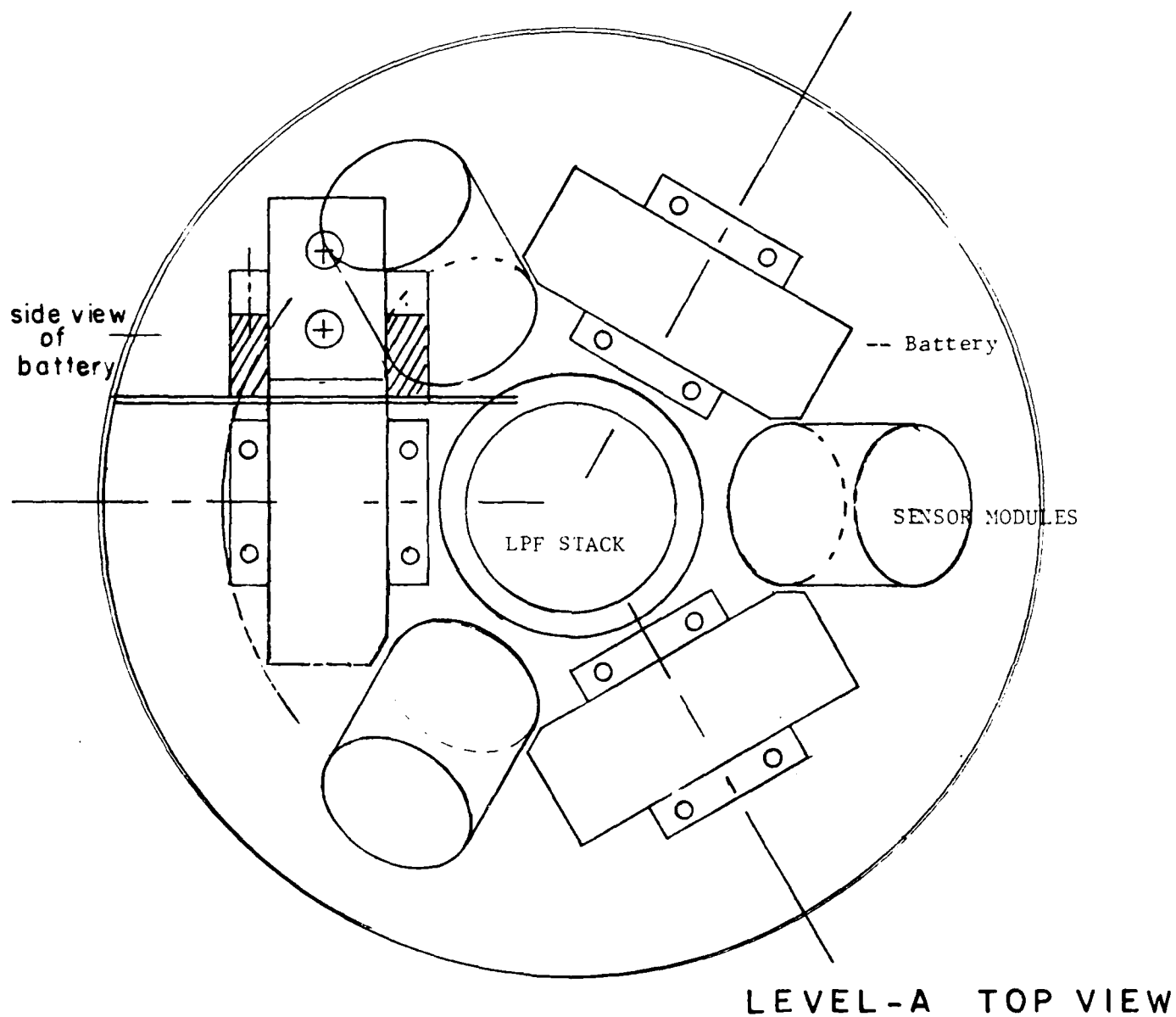Figure A9 - Layout of Sphere Modules seen from Center Level.

side view
of
battery

-- Battery

LPF STACK

SENSOR MODULES

LEVEL-A TOP VIEW

Figure A10 - Layout of Sphere Modules seen from mezzanine level about
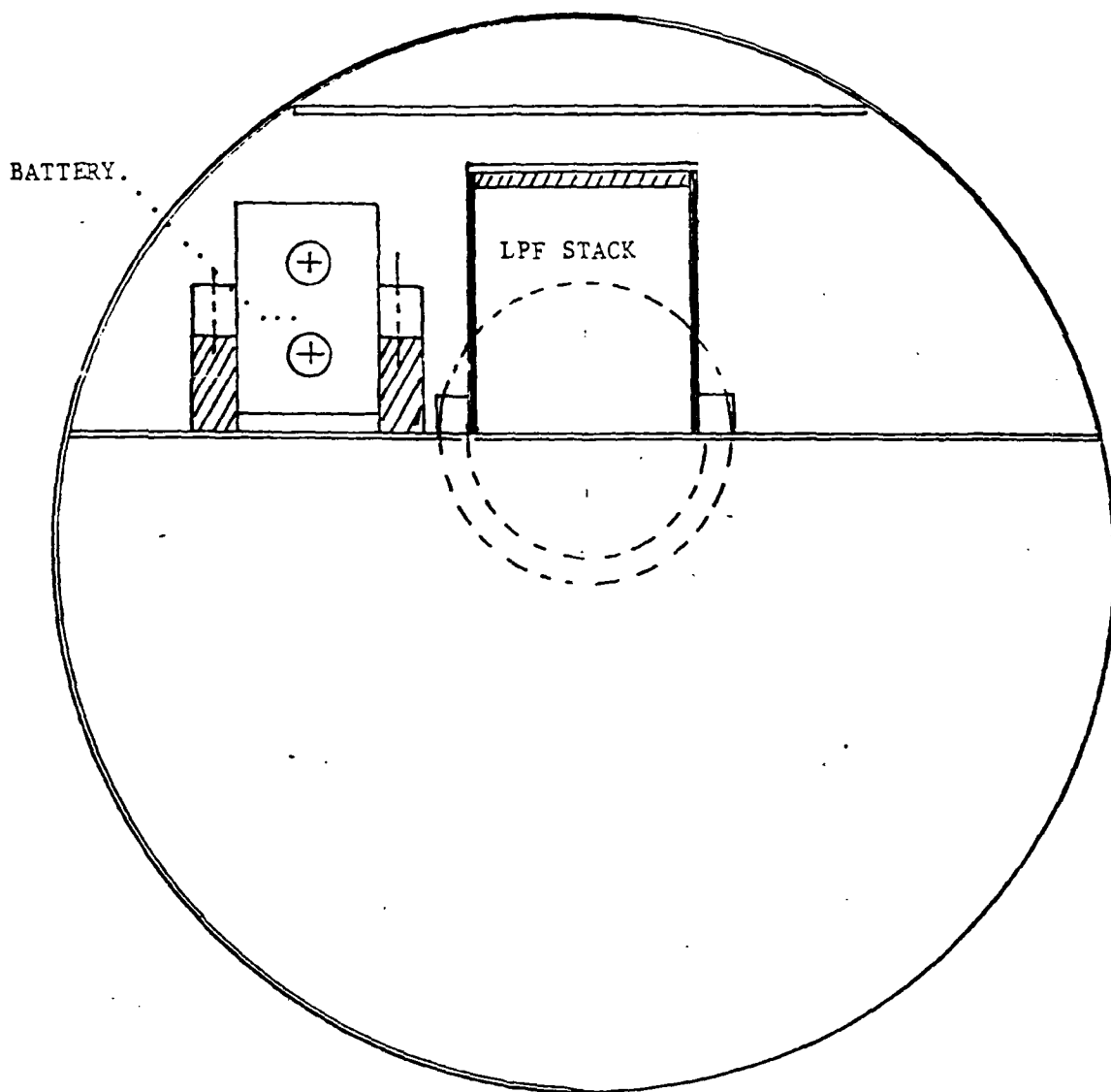2.5 cm up from center.

Figure A11 – Detail showing position of one of six batteries relative to Low pass filter stack in central core of sphere.